NAVAL POSTGRADUATE SCHOOL

MONTEREY, CALIFORNIA

THESIS

PRACTICAL APPLICATION OF RESIDUAL STRESS MEASUREMENTS ON MARITIME VESSELS

by

Dixon T. Whitley

June 2012

Thesis Advisor:	Luke Brewer
Second Reader:	Young Kwon

Approved for public release; distribution is unlimited

THIS PAGE INTENTIONALLY LEFT BLANK

REPORT DOCUMENTATION PAGE			*Form Approved OMB No. 0704-0188*
Public reporting burden for this collection of information is estimated to average 1 hour per response, including the time for reviewing instruction, searching existing data sources, gathering and maintaining the data needed, and completing and reviewing the collection of information. Send comments regarding this burden estimate or any other aspect of this collection of information, including suggestions for reducing this burden, to Washington headquarters Services, Directorate for Information Operations and Reports, 1215 Jefferson Davis Highway, Suite 1204, Arlington, VA 22202-4302, and to the Office of Management and Budget, Paperwork Reduction Project (0704-0188) Washington DC 20503.			
1. AGENCY USE ONLY ***(Leave blank)***	**2. REPORT DATE** June 2012	**3. REPORT TYPE AND DATES COVERED** Master's Thesis	
4. TITLE AND SUBTITLE Practical Application of Residual Stress Measurements on Maritime Vessels			**5. FUNDING NUMBERS**
6. AUTHOR(S) Dixon T. Whitley			
7. PERFORMING ORGANIZATION NAME(S) AND ADDRESS(ES) Naval Postgraduate School Monterey, CA 93943-5000			**8. PERFORMING ORGANIZATION REPORT NUMBER**
9. SPONSORING /MONITORING AGENCY NAME(S) AND ADDRESS(ES) N/A			**10. SPONSORING/MONITORING AGENCY REPORT NUMBER**
11. SUPPLEMENTARY NOTES The views expressed in this thesis are those of the author and do not reflect the official policy or position of the Department of Defense or the U.S. Government. IRB Protocol number _____N/A_____.			
12a. DISTRIBUTION / AVAILABILITY STATEMENT Approved for public release; distribution is unlimited			**12b. DISTRIBUTION CODE** A

13. ABSTRACT (maximum 200 words)

This thesis examines the practical application of portable X-ray diffraction to measure residual stresses on board active maritime platforms. These measurements will provide better understanding of structural failures in aluminum hulls and superstructures. The feasibility of this process was analyzed by comparing data from welded aluminum test samples using portable X-ray diffractometers from three different sources. The effects on residual stress from ultrasonic impact treatments were measured using laboratory X-ray diffraction. A comprehensive list of technical requirements for the purchase and deployment of a portable X-ray diffractometer was written. A case study for measurement of residual stresses on board a USN cruiser was developed.

14. SUBJECT TERMS X-ray diffraction, Aluminum, Ultra-sonic Impact Treatment (UIT), Residual Stress			**15. NUMBER OF PAGES** 99
			16. PRICE CODE
17. SECURITY CLASSIFICATION OF REPORT Unclassified	**18. SECURITY CLASSIFICATION OF THIS PAGE** Unclassified	**19. SECURITY CLASSIFICATION OF ABSTRACT** Unclassified	**20. LIMITATION OF ABSTRACT** UU

NSN 7540-01-280-5500 Standard Form 298 (Rev. 2-89)
Prescribed by ANSI Std. 239-18

THIS PAGE INTENTIONALLY LEFT BLANK

Approved for public release; distribution is unlimited

PRACTICAL APPLICATION OF RESIDUAL STRESS MEASUREMENTS ON MARITIME VESSELS

Dixon T. Whitley
Lieutenant, United States Coast Guard
B.S.E., University of New Mexico, 2004

Submitted in partial fulfillment of the
requirements for the degree of

MASTER OF SCIENCE IN MECHANICAL ENGINEERING

from the

NAVAL POSTGRADUATE SCHOOL
June 2012

Author: Dixon T. Whitley

Approved by: Dr. Luke Brewer
Thesis Advisor

Dr. Young Kwon
Second Reader

Dr. Knox Milsaps
Chair, Department of Mechanical and Aerospace Engineering

THIS PAGE INTENTIONALLY LEFT BLANK

ABSTRACT

This thesis examines the practical application of portable X-ray diffraction to measure residual stresses on board active maritime platforms. These measurements will provide better understanding of structural failures in aluminum hulls and superstructures. The feasibility of this process was analyzed by comparing data from welded aluminum test samples using portable X-ray diffractometers from three different sources. The effects on residual stress from ultrasonic impact treatments were measured using laboratory X-ray diffraction. A comprehensive list of technical requirements for the purchase and deployment of a portable X-ray diffractometer was written. A case study for measurement of residual stresses on board a USN cruiser was developed.

THIS PAGE INTENTIONALLY LEFT BLANK

TABLE OF CONTENTS

LIST OF FIGURES

LIST OF TABLES

THIS PAGE INTENTIONALLY LEFT BLANK

LIST OF ACRONYMS AND ABBREVIATIONS

AA5083	Aluminum Alloy 5083 H116
HAZ	Heat-Affected Zone
MIC	Metal Improvement Company
MIG	Metal Inert Gas Welding
SCC	Stress Corrosion Cracking
TEC	Technology and Energy Company
UIT	Ultrasonic Impact Technique
XRD	X-ray Diffraction

THIS PAGE INTENTIONALLY LEFT BLANK

ACKNOWLEDGMENTS

I would like to thank Professor Brewer for his exceptional hard work in guiding me through this process. His expertise on materials science, and as an advisor, provided me with an exceptional experience at the Naval Postgraduate School.

Thank you to Professor Kwon, and Professor Menon for giving me positive and helpful advice along the way and teaching me many of the details I needed for completing this work.

Thank you to LT Banazwski and LT Mattern. Their hard work was the basis of this thesis, and their dedication in helping me made this possible.

I received great support and information for this project from Dr. Kim Tran, and William Goins from the U.S. Navy.

Key information was provided by the Metal Improvements Company, Proto Manufacturing, and the Technology for Energy Company. The time and energy provided by their staffs showed the greatest professionalism and was invaluable to my work and learning experience.

THIS PAGE INTENTIONALLY LEFT BLANK

I. MOTIVATION

Current trends showing a rising cost in energy and the ever present movement of the military services to fewer and more capable vessels has created great interest in moving to lighter, faster, and more fuel efficient vessels. The easiest way to gain this efficiency is by reducing the overall weight of the vessel. To get a reduction in weight without reducing functionality, the strategy has been to replace structural components that were traditionally made out of steel with aluminum, which has about 1/3 of the density. This approach has led both the military and some commercial marine vessel builders to start creating vessels out of aluminum either in part or in whole, e.g., Navy cruisers, high speed surface vessels, and littoral combat ships. This achieved reduction in weight makes the vessel faster, travel farther, or reduce its fuel consumption. Calculations done by Mattern show the three way trade-off between range, fuel, and speed of a typical marine vessel with a 15% reduction in weight [1], Figure (1).

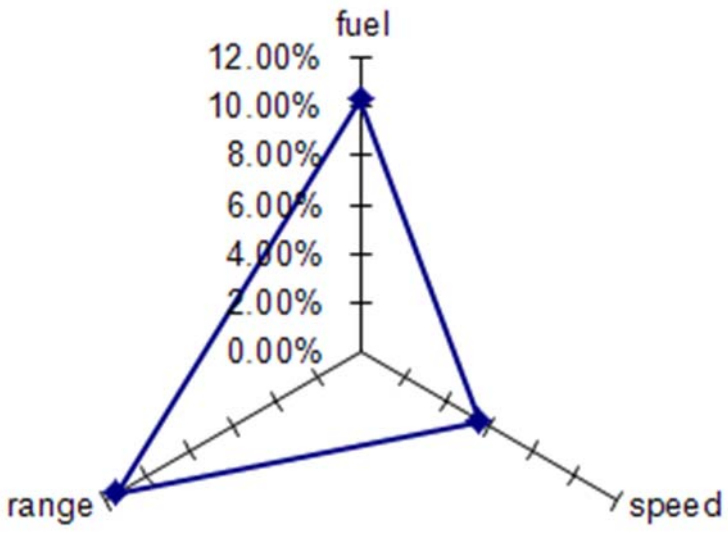

Figure 1. Fuel consumption to speed to range for 15% reduction in weight for a naval vessel. After [1]

The U.S. Navy spent around $14 billion a year on total fuel costs since 2006 compared to an average of about $6 billion per year between 1992 and 2004 Figure (2)

[2]. This drastic increase in fuel is driving the U.S. Navy to invest heavily to increase fuel efficiency. This change also changes the economy of constructing new ships, with money spent in making new vessels lighter will have a real and compelling long term monetary incentive to spend more money to move to vessels made of aluminum and composite hulls.

Figure 2. DoD expenditures on fuel compared to overall fuel consumption. After [2]

In addition, a large variety of commercial ships, mostly ferry boats and small to medium sized passenger vessels, are built out of aluminum. As of 2009, the Benchihjigua Express is the largest commercial aluminum ship at 112 meters [3]. The U.S. Navy has also increasingly moved to aluminum super structures on cruisers, and is currently building Littoral Combat ships using both steel with Aluminum superstructures and all aluminum ships Figure (3). The Navy's concept design of the high speed vessel HSV-2 is a converted car carrier with an aluminum hull [3].

Figure 3. LCS 2 Steel mono hull with aluminum superstructure. Official U.S. Navy photo.

While aluminum has major advantages for naval structures it is also worth examining why it has taken so long for ship builders to widely adopt aluminum and why so many ships are still built with steel. The major advantage of aluminum is its low density in comparison with steel, and its overall cost advantages over carbon composite. These advantages and disadvantages are shown in Table (1). Within the family of aluminum alloys there are three major choices of materials 1000 series, which are mostly pure aluminum, high strength aluminum 2000 and 7000 series most commonly known for use in aircraft, and 5000 series aluminum. A comparison of these alloys is shown in Table (2).

Table 1. Properties of materials for use in naval structures.

	Possible Hull and Superstructure Materials				
Material	Density g/cm^3	Corrosion	Joining and Repair	Stiffness	Cost
Al	2.7	Good	Difficult	Moderate	Moderate
Steel	7.85	Moderate	Excellent	High	Low
Fiber Composites	1.5-2.0	Very Good	Difficult	Low	High

Table 2. Comparison of types of aluminum alloys.

	Aluminum			
Material	Strength	Corrosion	SCC	Welding
Pure AL	Inadequate	Excellent	N/A	Not Weldable
Hight strenght AL	Good	Moderate	Poor	Not Weldable
5XXX series AL	Moderate	Good	Moderate	Weldable

Table (1) shows that aluminum and carbon composites both have significant advantages in both density and corrosion properties. In the past, advantages were largely offset by the relatively low cost of fuel, and by the excessive extra cost of joining aluminum and carbon structures. With recent increases in world fuel costs, more governments and companies are willing to face these challenges. 5xxx series aluminum can be welded but faces a number of difficult and expensive conditions and with a much larger and potentially more dangerous set of side effects than steel. Porosity from hydrogen bubbles and the high thermal expansion coefficient of aluminum tends to lead to high residual stresses and subsequent cracking at the welds. These problems, along with the general loss of strength in moving from steel to aluminum, lead to a number of design problems. Making up this loss of strength with more material undermines the aim for reduced weight; so much more care must be taken on how stress is applied to the structure.

Another major issue in using aluminum or composite materials compared with steel is the relatively poor high heat performance of these materials. Aluminum has a melting point of 660 degrees C versus 1500 degrees C for steel. This makes an aluminum hull or superstructure vulnerable to damage when subjected to a major internal fire. There

are two major USN cases where this has happened. The first was the USS Belknap CN-23, which collided with the aircraft carrier JFK in 1975. The subsequent fire resulted in the collapse of the vessels superstructure. The USS STARK was hit by an Exodent missile in 1987, but the vessel survived the subsequent fire. Modern use of fire insulation on naval aluminum mitigates this effect to a large degree. Weight of the additional insulation for use on aluminum ships takes approximately 40% more weight than insulation on steel but still results in a weight savings of around 22% [4]. This combined with better automated fire protection systems negate the worst of the fire protection concerns in using aluminum.

Figure 4. USS Belknap after collision with USS John F. Kennedy in 1975. Official U.S. Navy Photo.

The third major design problem moving to non-ferrous structures in stiffness of the material. Steel is roughly three times stiffer than aluminum, and composite materials are inherently anisotropic so while they may be stiff in one direction they are much more complaint in orthogonal directions. Deflections in a 50-meter long composite ship will have hull deflection as much as 300% greater than a steel vessel of the same design [5].

This will cause significant design problems with fatigue cracking and in keeping sensitive systems aligned. With aluminum the same problem exists, but to a lesser degree. This problem is a large contributor in what has been keeping all aluminum hulled ships to relatively small vessel designs. Large deflections become a much bigger problem when put on ships over 100 meters and are designed to sail in heavy seas. Using nonferrous metals on the superstructure, but not the hull, relieves most of this problem.

The ability to join materials in the construction and repair of a marine vessel is a large driving factor in both construction and operating costs. A major factor in the dominance of steel over the last 150 years has been its relative ease to which it can be joined without unacceptable losses to its material properties. While there are a large number of possible problems that can occur with the welding of most commercial steels, these can be mostly overcome in a cost effective manner. Many kinds of aluminum cannot be effectively welded due to high thermal expansion, and high hydrogen induced porosity that leads to highly brittle microstructures and fracturing. A major factor in the use of 5000 series aluminum vice higher strength series such as 2000 or 7000 series aluminum is that it can be welded, although with greater difficulty and therefore greater expense than steel. Composites cannot be welded and therefore must be joined by other means such as using adhesives or riveting that is inherently more expensive, less reliable, and with higher chances of fatigue-related failure than welding.

Corrosion is a major cost factor when designing any marine vessel. Sea water is exceptionally corrosive and most metals exposed to it will undergo electro-chemical oxidation. The iron in steel is highly corrosive and undergoes a significant rate of corrosion. Painting and use of sacrificial anodes can reduce the worst of these effects but not all of it. While aluminum is easily oxidized it creates a coating of aluminum oxide that is difficult to penetrate, effectively protecting the underlying material from further corrosion. However, pure aluminum does not have sufficient strength to be used a structural material unless it is alloyed with copper, zinc or magnesium. While these alloys still have reasonably good overall corrosion characteristics they are all vulnerable to some degree to stress corrosion cracking [6]. The degree of susceptibility to this is

another reason that 5000 series aluminums are used for marine functions. While 5000 series aluminum has the required strength and while it is vulnerable to SCC it retains enough resistance to be useable.

The last and most compelling difference in materials is cost. Steel construction is the easiest and most cost effective method of ship construction. In the past, ship construction cost has been the dominant pricing factor for nearly all design choices on both navy and commercial ships. Composite construction costs would increase cost between 18–140% for replacing the superstructure of a naval ship [5] compared to approximately 7.5% for aluminum [7]. Continued advances in fabrication and welding will make improve both the prices and performance of both aluminum and carbon composite materials and with this increased range of applications on larger vessels. With the combination of the cost, corrosion, joining, and stiffness of the available materials 5000 series aluminum is the logical and compelling choice using current technology.

A. PROBLEMS WITH ALUMINUM STRUCTURES

1. Fatigue Cracking

Aluminum structures are heavily prone to cracking from simple fatigue loading. The majority of cracks found in aluminum arise from cyclic loading that over repeated cycles causes brittle failure from loads much lower than the materials ultimate or yield strength. 90% of all metal failures come from fatigue [6]. Cracks will be initiated at a stress riser such as a weld toe, scratch or bolt and grow as the repeated stress placed on the vessel slowly grows the crack to its critical length [6]. Marine vessels moving through the ocean are subject to consistent cyclic stress and the large number of welds and other joins creates large numbers of areas with high residual stresses where these cracks can start.

Unlike steel, aluminum does not have a clear fatigue endurance threshold. This is normally defined as the stress level at which a metal can endure more than 10 million cycles without cracking or failing. In aluminum structures, there is no clear stress below which the material can be shown to not fail [6].

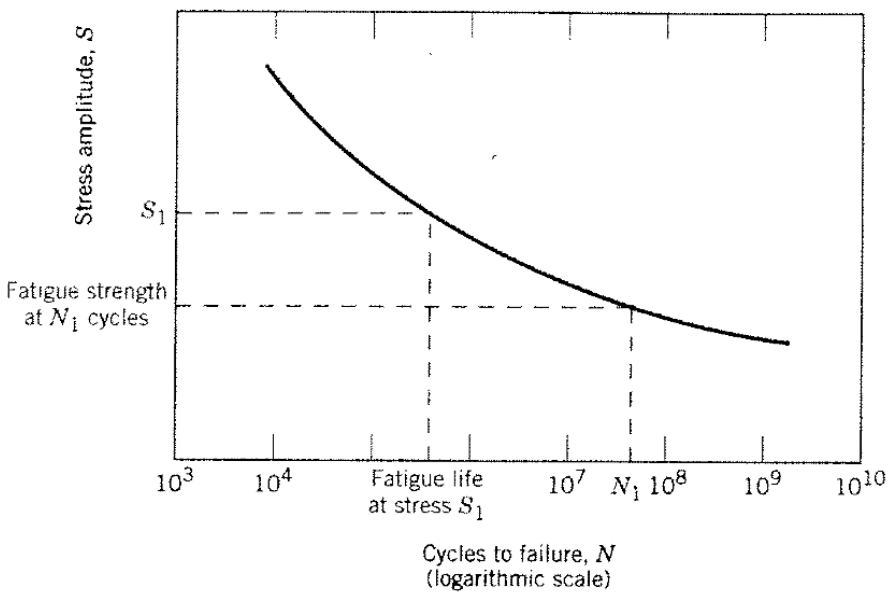

Figure 5. Stress versus cycles to failure. After [6].

While there are many stresses that a ship is subject to from vibrations of the engine to work loading from the crew, the main stress that most heavily affects the bulk of the hull and superstructure is the hogging and sagging of the vessel from moving through the ocean. The hogging and sagging of the vessel act as a minimum and maximum stress for the structure.

$$\sigma_m = \frac{\left(\sigma_{\max} + \sigma_{\min}\right)}{2} \tag{1}$$

$$R = \frac{\sigma_{\min}}{\sigma_{\max}} \tag{2}$$

$$\sigma_a = \frac{\left(\sigma_{\max} - \sigma_{\min}\right)}{2} = \frac{\sigma_r}{2} \tag{3}$$

$$\sigma_a = \sigma_{fat}\left[1 - \frac{\sigma_m}{\sigma_{ut}}\right] \tag{4}$$

Equations 1 through 3 show the basic calculations for finding the mean stress, σ_m, stress ratio R, the stress range σ_r, the ultimate tensile stress σ_{ut} and stress amplitude σ_a, by knowing what the minimum and maximum stresses are σ_{min} and σ_{max}.

Equation 4 is called the Goodman equation and will estimate change in fatigue stress for constant fatigue life given a change in mean stress. For a naval vessel this means that either a higher (more tensile) average stress on the structure or higher difference range of stresses negatively affect the vessels fatigue life. So a higher mean stress left by residual stress will significantly reduce the number of cycles to failure for the given material [8]. This can cause difficulties for a naval vessel as the degree and range of stresses it is subjected to can vary significantly on the operating environment it is subjected to. Another important aspect from the Goodman relationship is that negative stresses also affect the fatigue life of the material. As any residual stress either from welding or a peening process designed to reduce vulnerability from residual stress will add to the mean stress of the structure and therefore reduce the fatigue life of the material.

2. Stress Corrosion Cracking

One of the more serious and problematic failure modes seen on aluminum structures in stress corrosion cracking (SCC). This occurs when a sensitized aluminum structure is placed in a corrosive environment and then placed under tensile stress. Unfortunately, 5000 series aluminum on marine platforms faces all three of these challenges. 5000 series aluminum alloys that are used on the Navy LCS and cruisers have between 4.5 and 5.7% magnesium. For materials with magnesium contents greater than 3%, the solid solution is not stable; and if given enough thermal energy, the solution will separate into separate phases [9]. For 5000 series aluminums, temperatures above 50 degrees C over an extended period of time (many years) will cause the magnesium to separate out from its solid solution and to form beta precipitates (Mg_2Al_3) along the grain boundaries. This process sensitizes the metal as this beta phase is much more prone to corrosion than the surrounding metal. When this beta phase comes into contact with seawater it corrodes much more rapidly than the surrounding material leading to

structural weakness along the grain boundaries. When a tensile stress is applied, the loss of strength and ductility from this targeted corrosion makes the material susceptible to intergranular cracking Figure (6).

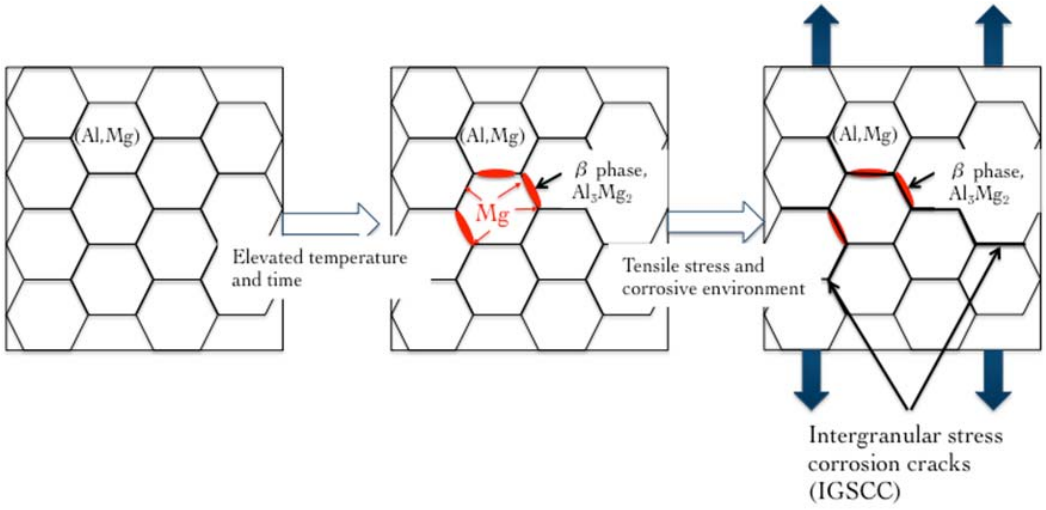

Figure 6. The formation of Beta phase sensitizing aluminum.

To get SCC requires three simultaneous conditions: a susceptible metallurgy, a corrosive environment and tensile stress. If any one of these three factors in eliminated then the material failure will be avoided. The use of high Magnesium concentration is desirable as it provides the needed high strength for aluminum structures. The corrosive environment is an unavoidable aspect of operating in the ocean. Attempts to mitigate this problem have focused upon reducing the tensile stresses that the material faces. Applied stresses to the ship include stress from the waves, wind and the propulsion of the vessel as well as hogging and sagging. Residual stresses include stress from welding, riveting and bolting of structural members.

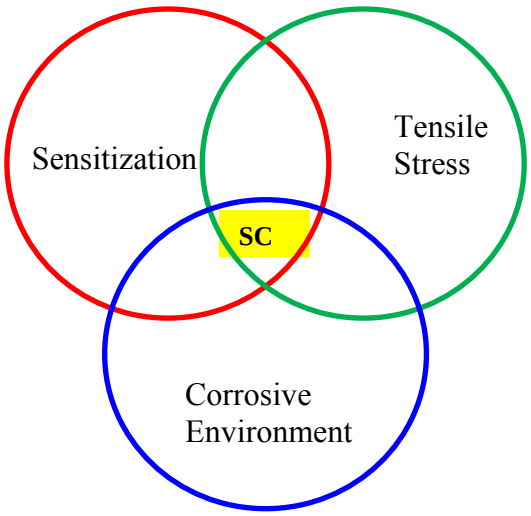

Figure 7. Venn diagram depicting causes of SCC. After [1].

SCC has been found in areas that have tensile stresses from both residual stress and from fatigue stress. Common places that have been observed are around welds, bolts, rivets, as well as areas of vessels that are subject to hogging and sagging from wave and wind action as well as other areas where the large stress fields are somewhat less apparent. In 2001 and 2002, over 400 commercial vessels built out of 5083-H321 aluminum began to experience SCC, as well as severe pitting, leading to many being unfit for service. Shown in Figure (8), this was caused by the aluminum plate from a manufacturer becoming sensitized before installation [10].

Figure 8. SCC cracking in commercial vessel engine room. After [1].

The U.S. Navy's Ticonderoga class cruisers have also had severe SCC in the aluminum superstructure. Large numbers of extensive cracks up to several feet long have occurred throughout the structures including areas where no obvious stress risers are present, such as in deck plating or in the middle of bulkheads. Over 3,000 cracks have been reported costing $14 million for the repair of one USN cruiser alone [11].

II. INTRODUCTION

A. CAUSES OF RESIDUAL STRESS

Residual stress is a stress that is left over from a process that leaves either a tensile or compressive strain within a material, existing as a constant stress state without the application of an outside force. Residual stress on ships commonly comes from joining processes such as welding, riveting and bolts leaving large residual tensile stresses. For aluminum, the high thermal stress from fusion welding is especially challenging. When a metal is welded, the increased heat causes the metal pieces to expand around the heat affected zone (HAZ). For fusion welding, the metal at the weld line is heated until it melts. When weld-line cools and solidifies, the surrounding metal also cools and contracts. If the metals being joined are constrained in their movements, this contraction will result in both tensile and compressive stresses within the structure [12]. This problem is particularly difficult when dealing with aluminum as its thermal expansion coefficient is about 1/3 higher than that of steel implying significantly greater resultant stresses in aluminum versus steel when aluminum is already has a much smaller resistance to fracture. These stresses can be calculated as a function of the distance from the weld centerline, defined as y, using Equation 5 so long as the maximum residual stress and width of the tension zone are known [13].

$$\sigma_x(y) = \sigma_m \left[1 - \left(\frac{y}{b} \right)^2 \right] \exp\left[-\frac{1}{2} \left(\frac{y}{b} \right)^2 \right] \tag{5}$$

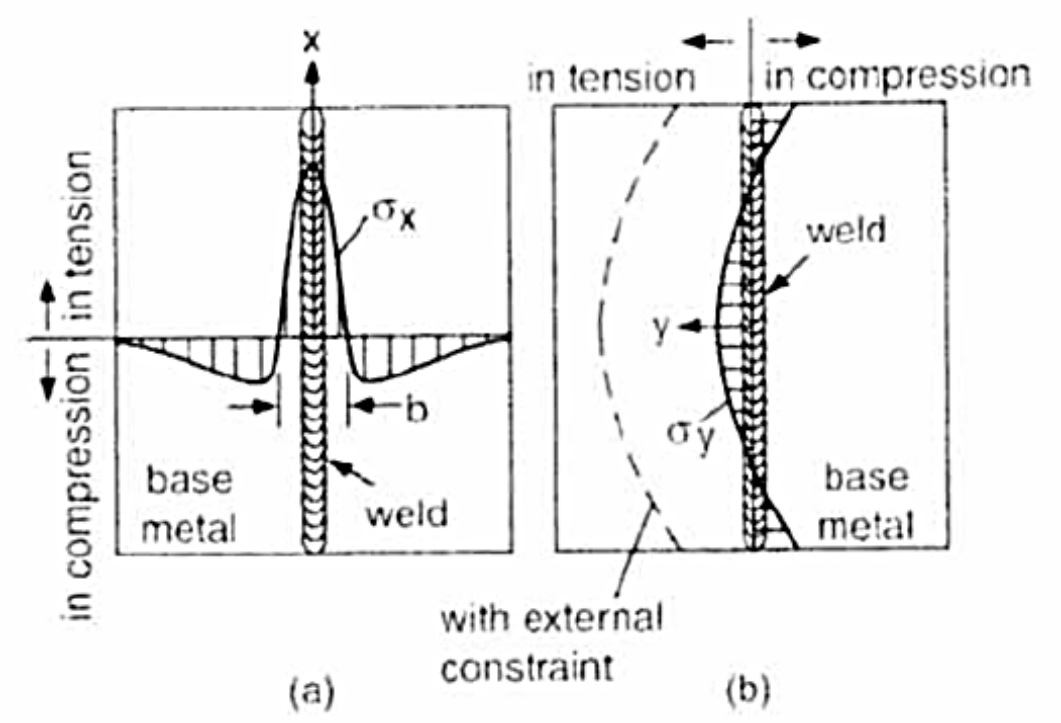

Figure 9. Typical residual stress distributions along vertical and horizontal directions. From [13].

Figure (9) shows that along a the surface of a fusion weld the stress is compressive right at the weld centerline then quickly becomes in tension on either side of the welds path. Looking at the stress in the vertical direction along the fused material, this compressive stress is only at the surface of the material, as you go deeper into the center of the material the stress is again in tension. This is due to the way the material solidifies and cools with the surface of the material cooling at a faster rate than the center pulling the surface of the material towards the center of the weld creating compression at the surface and tension at the center.

Figure (10) compares measured residual stresses to a finite element model as a function of the distance from the weld centerline parallel from the weld centerline to the end of one side of the newly welded plate defined as a distance W. This example demonstrates residual stresses that are over 10% above the nominal yield stress near the weld centerline. This result clearly demonstrates the high degree of residual that can be caused by fusion welding [13].

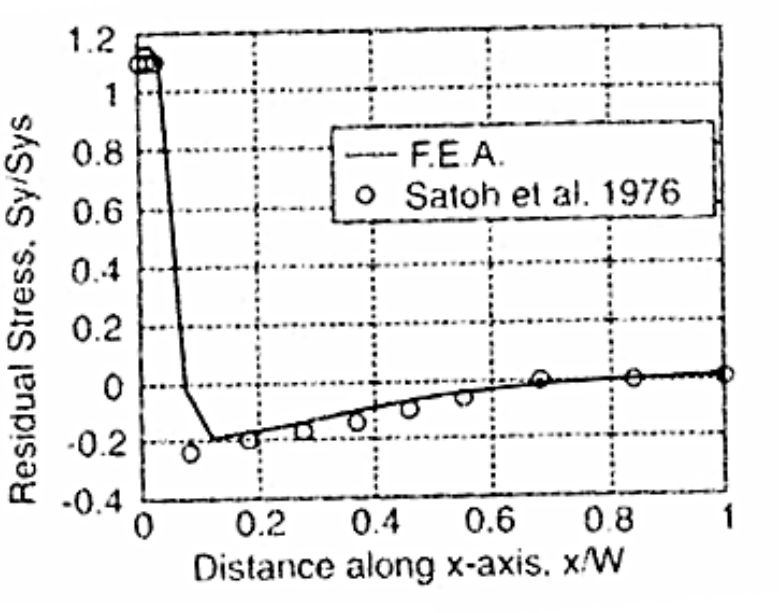

Figure 10. Measured and predicated residual stress in weld. From [13].

James et al. used synchrotron diffraction to measure residual stresses that resulted from gas-metal arc welding in 5083 aluminum [14]. Synchrotron diffraction uses a high-energy X-rays (>50keV) that can penetrate deeper into the sample and are more sensitive than normal laboratory X-ray diffraction. This study showed peak longitudinal stresses of 80 to 90 MPa at around 20 mm from the weld centerline. This peak stress occurs outside of the edge of the HAZ, which was shown to end 12 mm from the weld centerline. The transverse stress was tensile through the entire cross section of the plate [14]. This technique also allowed for the measurement of the stress at varying depths within the material. The residual stresses continued at very comparable values for several mm inside of the metal.

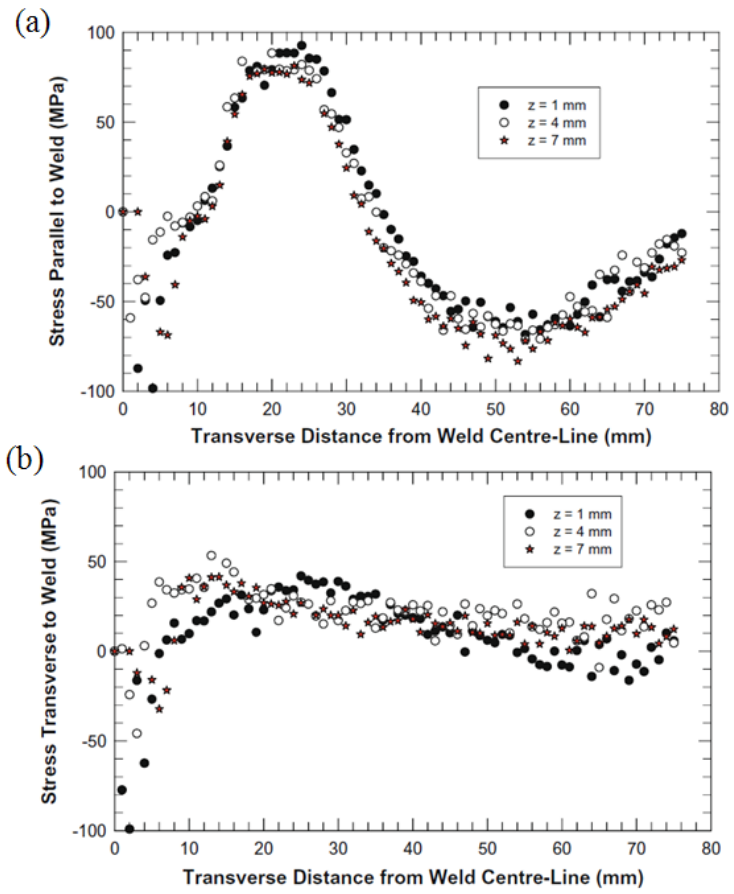

Figure 11. (a) longitudinal stresses at 1, 4 and 7 mm in 5083 aluminum (b) transverse stresses at depths of 1, 4 and 7 mm in 5083 aluminum. From [14].

Residual stress has also been demonstrated to have a negative effect on the fatigue life of welded metals. In Figure (12), the cyclical mean stress versus number of cycles to failure is shown for AA5083, comparing welded metal in both air and seawater environments. This graph clearly shows that welding of aluminum drastically decreases it maximum fatigue loading by between 35–65% [15]. It is key to note that there are two causes of this loss in fatigue life, both residual stresses and changes in microstructure due to the melting and solidifying of the metal. There is no clear way to accurately separate out these effects from each other [15], and as the effects will ultimately go hand-in-hand, and the combined result is of greater interest.

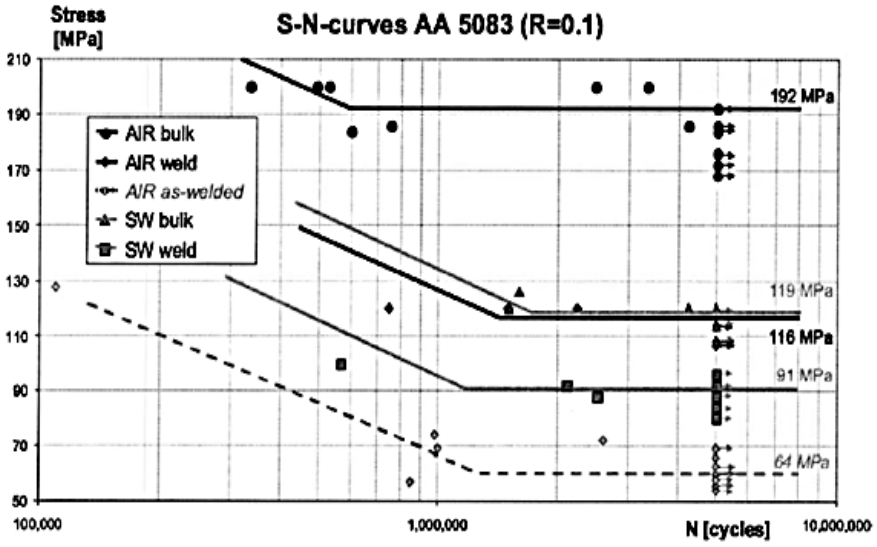

Figure 12. SN curve and fatigue limits of 5083 aluminum comparing un-welded metal to samples welded and exposed to air, and seawater. From [15].

B. PEENING PROCESSES

Reducing the tensile stress at the surface of a metal is a key factor for avoiding fatigue and stress corrosion cracking. The most successful method is to induce a surface compressive stress on the metal. This compressive stress is often created by plastically deforming the metal surface using one of several peening processes. Applying peeing to weld surfaces has been shown to significantly improve service fatigue life for traffic fixtures at minimal cost [16].

Shot peening is a process that uses small hard glass particles from .1 to 1 mm that are shot using a compressed gas at high velocity onto the treated surface. The resulting impact will deform the metal's surface leaving a compressive residual stress on the surface. This resulting stress will go to a depth of about 25 to 50% of the diameter of the particle that is being used [6]. Average depth of this method is about 250 μm, which tends to be too shallow for practical prevention of SCC. It is also very hard to get full coverage of the area due to the fact that the projected particle pattern is completely random leading to inconsistent results. The advantage to this method is that it is relatively cheap to use and fairly easy to find the equipment and training to run.

This method uses continuous ultrasonic vibrations transferred through a high strength, high hardness tool that continuously impacts the treated surface. This high frequency hammering of the material creates a near-surface high zone with severe plastic deformation. The resulting compressive stresses have been shown to penetrate as far as 1mm into the material [17] (see Figure (13).

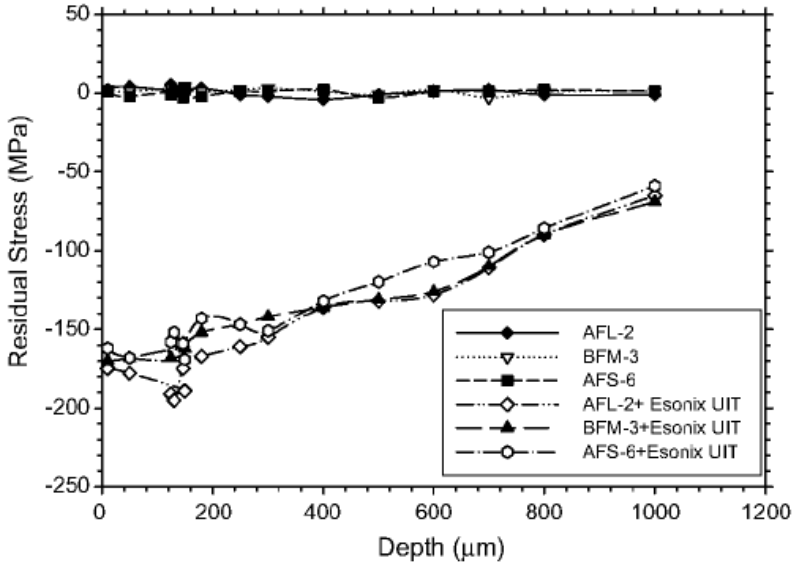

Figure 13. Residual stress distribution for Esonix UIT treatment on lightly, moderately and severely exfoliated 7075 aluminum. From [17].

Clear positive effects of fatigue life from peening process have also been shown. Field studies at UT Austin have shown clear fatigue life benefits in UIT treating repaired traffic signals under cyclic stress from wind action [16] Tran et al investigated the fatigue life of lightweight alloys that had been laser peened. These experiments showed that using a four point bending test significant increase in fatigue life could be reliably demonstrated on 5059 aluminum and MP35 N high nickel alloy [18].

Use of UIT treatments to impart residual stresses while generally less effective than laser peening [19] UIT treatment has a number of practical advantages that make it highly desirable. The equipment and process used in laser peening is expensive and the need for an even flow of electrolyte makes it difficult to use for many practical applications. In contrast, UIT systems are relatively cheap, portable do not create any

waste and relatively simple to use. Figure (17) shows workers in Austin TX performing field UIT treatments to a steel traffic signal to combat fatigue damage caused by persistent winds in the area [16]. This simple quick procedure done during routine maintenance would be impractical to perform with laser peening.

Figure 14. UIT impact treatments being applied to a traffic signal in Austin TX. From [16].

Laser peening uses a high intensity laser beam to create a compressive stress similar to that created by shot peening and UIT. The laser is often a high energy neodymium glass laser that sends a pulse of energy that impacts the surface turning a localized piece of the surface into plasma. By applying a tamping layer, normally flowing water, this plasma will become laterally confined causing a buildup of pressure up to several GPA at the surface of the material [18]. The shock wave caused by this pressure build up plastically deforms the material leaving a large compressive residual stress in the material Figure (14). This is done with minimal thermal loading and the temperature only rises to around 149 degrees C. This process leaves a relatively smooth surface as compared to shot peening or UIT, which is desirable when the surface needs to be repainted. This technique also allows for much greater control of how much compressive stress is put into the material. Laser power, target spot size, pulse duration and the confining medium are all easier to control and can achieve results to as much as 10 times as deep as shot peening [19].

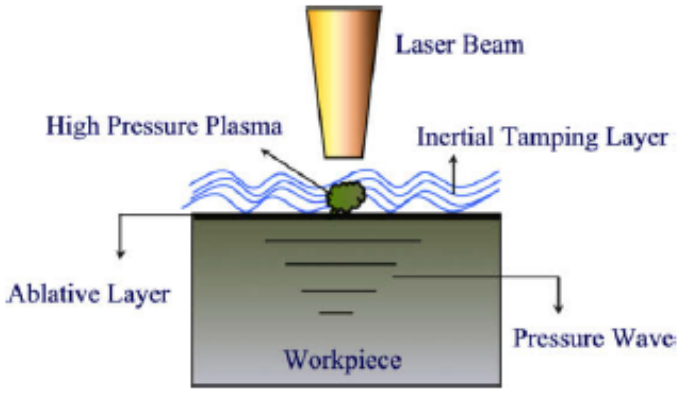

Figure 15. Laser Peeing Process. From [19].

Laser peening processes have been shown to have dramatic impact on preventing SCC and improving fatigue life. Figure (16) demonstrates the dramatic impact that laser peening can have on a structure. Note how the cracks arrest when it reaches the peened region. Hamtamleh studied the SCC behavior of shot and laser peened behavior in 2195 aluminum using a slow strain rate test in a corrosive environment clearly demonstrating which clearly showed that laser peened samples outperforming unpeened and shot peened samples.

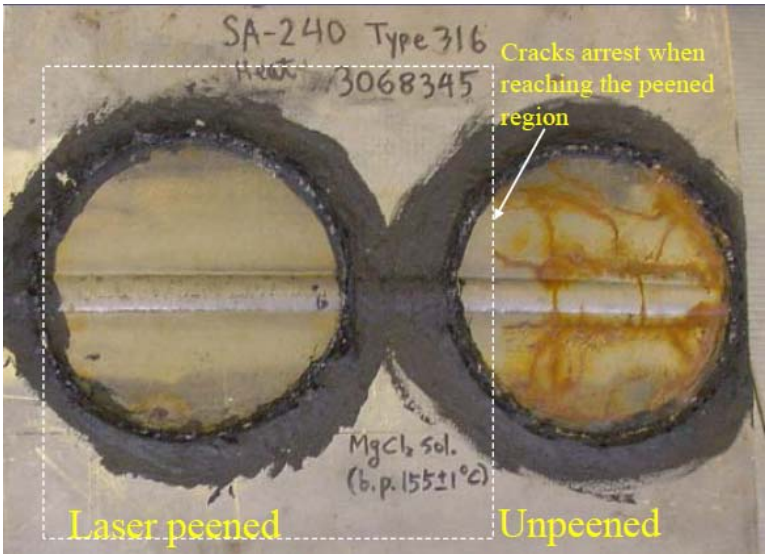

Figure 16. Corrosion testing of 316 stainless steel. Tank with welds was partially laser peened at Lawrence Livermore National Laboratory as part of a high-level waste program (Francis T. Wang et al., LLNL). Figure provided by the Metal Improvement Company.

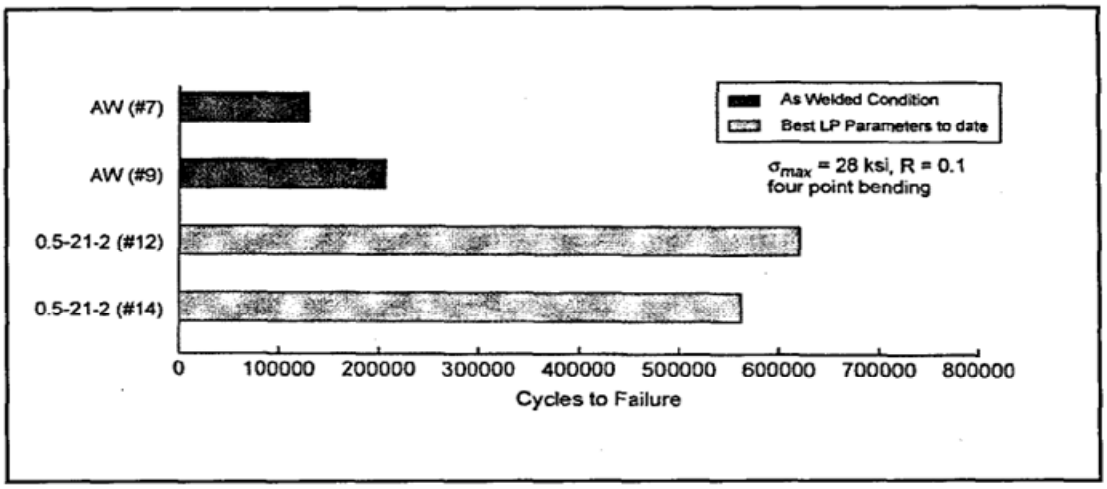

Figure 17. Four point bending test for laser peened welded aluminum. From [18].

C. X-RAY DIFFRACTION

1. Background

X-ray diffraction (XRD) has become one of the most common methods for measuring residual stress over the last few decades [20]. This method measures the strain in the crystal structure, and stress can be calculated. In X-ray diffraction, the d-spacing in the crystal structure can be measured and compared to that materials unstressed state by looking at the shift in the diffraction peak angle. This will give a strain value, which using Hooke's law can be converted into a stress value [21]. To find this d-spacing, a number of physical properties of the metal must be known. The 2theta or Bragg angle for each individual reflection plane for material and type of radiation must be known. For aluminum, copper, chromium and cobalt tubes are most commonly used. The choice of a reflection at a diffraction angle, 2θ that is as high as possible gives a better result as high angle diffraction peaks are more sensitive to the effects of elastic strain. For copper X-ray tubes {422} {331} and {420} reflections are common, and for Chromium tubes common reflections are {311} and {222}.

The strain is found by using Bragg's law of diffraction. Bragg diffraction occurs when an X-ray beam hits a crystalline structure Figure (18). Constructive and destructive interference between entering and exiting waves occur inside of the crystal, producing

diffraction patterns with peaks of intensity at specific angles. Bragg found that the angle that these diffracted beams come out are dependent on the space between the atomic layers of the crystal structure (d-spacings) and the wavelength of the radiation that is used [22].

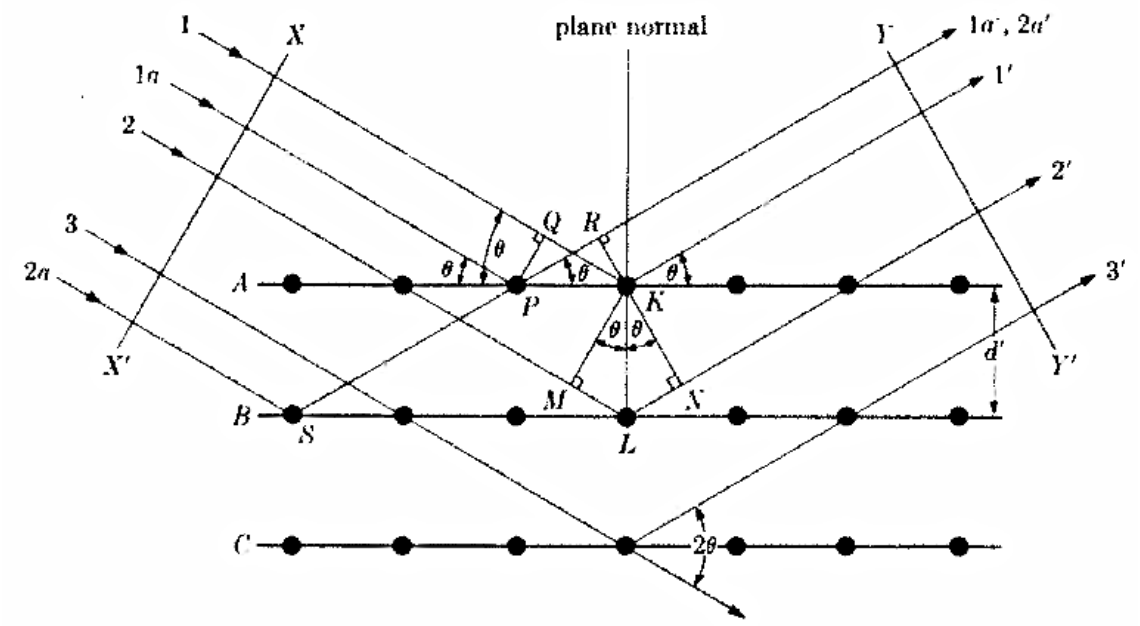

Figure 18. Demonstration of Bragg's Law. From [22].

Braggs law Equation (7) shows this relationship when λ is the wavelength, d is the crystal lattice spacing and θ is the angle of diffraction.

$$\lambda = 2d \sin\theta \tag{7}$$

As the incident X-ray wavelength is a known quantity, and the 2θ angle from the centroid is found by finding the center of the diffraction peak angle, the lattice spacing or d can be calculated. For any reflection set {hkl}, a unit cell parameter can be found by using Equation 8.

$$d = \frac{a}{\sqrt{h^2 + k^2 + l^2}} \tag{8}$$

The change in d-spacing can be measured at different orientations by rotating the sample in the ψ direction. If there is a direction change in the d spacing as the ψ angle changes, then the 2θ angle will change and a different d_ψ is found. A sample with elastic change will systematically change in the measured d-spacing as a function of ψ tilt. In this way the crystal lattice is acting a strain gauge and can be utilized in much the same way.

Once the d-spacing is measured, the measured strain can be determined. Using a known initial d-spacing d_0 and a measured $d_{\phi\psi}$ (d-spacing for a given ψ and ϕ angle), the strain can be measured using Equation 9 [20].

$$\left(\varepsilon_{33}^{'}\right)_{\phi\psi} = \frac{d_{\phi\psi} - d_0}{d_0} \tag{9}$$

By repeating this experiment for a series of ψ and ϕ angles, a full 3-D strain tensor can be calculated. A minimum of six independent measurements are needed for this to account for the six unknowns in Equation 10.

$$\left(\varepsilon_{33}^{'}\right)_{\phi\psi} = \frac{d_{\phi\psi} - d_0}{d_0} = \varepsilon_{11}\cos^2\phi\sin^2\psi + \varepsilon_{12}\sin 2\phi\sin^2\psi + \varepsilon_{22}\sin^2\phi\sin^2\psi + \varepsilon_{33}\cos^2\psi + \varepsilon_{13}\cos\phi\sin 2\psi + \varepsilon_{23}\sin\phi\sin 2\psi \tag{10}$$

The resulting strain tensor matrix can be determined using basic linear algebra will the linear system of equations in Equation 11.

$$A\cdot\vec{x} = \vec{b} \tag{11}$$

Solving for this equation and combining with Equation 10 leads to.

$$\begin{pmatrix} \left(\varepsilon_{33}^{'}\right)_{\phi_1\psi_1} \\ \left(\varepsilon_{33}^{'}\right)_{\phi_2\psi_2} \\ \left(\varepsilon_{33}^{'}\right)_{\phi_3\psi_3} \\ \left(\varepsilon_{33}^{'}\right)_{\phi_4\psi_4} \\ \left(\varepsilon_{33}^{'}\right)_{\phi_5\psi_5} \\ \left(\varepsilon_{33}^{'}\right)_{\phi_6\psi_6} \end{pmatrix} = \begin{bmatrix} a_1 & b_1 & c_1 & d_1 & e_1 & f_1 \\ a_2 & b_2 & c_2 & d_2 & e_2 & f_2 \\ a_3 & b_3 & c_3 & d_3 & e_3 & f_3 \\ a_4 & b_4 & c_4 & d_4 & e_4 & f_4 \\ a_5 & b_5 & c_5 & d_5 & e_5 & f_5 \\ a_6 & b_6 & c_6 & d_6 & e_6 & f_6 \end{bmatrix} \begin{pmatrix} \varepsilon_{11} \\ \varepsilon_{12} \\ \varepsilon_{13} \\ \varepsilon_{22} \\ \varepsilon_{23} \\ \varepsilon_{33} \end{pmatrix} \tag{12}$$

where

$a_i = \cos^2\phi \sin^2\psi, b_i = \sin 2\phi \sin^2\psi, c_i = \sin^2\phi \sin^2\psi, d_i = \cos^2\psi,$

$e_i = \cos\phi \sin 2\psi,\ f_i = \sin\phi \sin 2\psi \quad and \quad i = 1:6$

Now that the strain values are known the stress values can be calculated using the general form of Hooke's law. Where G is the bulk modulus, E is Young's modulus and ν is Poisson's ratio.

$$\begin{pmatrix} \sigma_{11} \\ \sigma_{22} \\ \sigma_{33} \\ \sigma_{23} \\ \sigma_{13} \\ \sigma_{12} \end{pmatrix} = \begin{bmatrix} 2*G+\lambda & \lambda & \lambda & 0 & 0 & 0 \\ \lambda & 2*G+\lambda & \lambda & 0 & 0 & 0 \\ \lambda & \lambda & 2*G+\lambda & 0 & 0 & 0 \\ 0 & 0 & 0 & G & 0 & 0 \\ 0 & 0 & 0 & 0 & G & 0 \\ 0 & 0 & 0 & 0 & 0 & G \end{bmatrix} \begin{pmatrix} \varepsilon_{11} \\ \varepsilon_{22} \\ \varepsilon_{33} \\ \varepsilon_{23} \\ \varepsilon_{13} \\ \varepsilon_{12} \end{pmatrix} \tag{13}$$

$$\lambda = \frac{E+\nu}{(1+\nu)*(1-2\nu)} \tag{14}$$

$$G = \frac{E}{2(1+\nu)} \tag{15}$$

So, from six different X-ray diffraction readings on one point, the full tensor residual stress can be calculated.

Use of Portable XRD devices to Measure Residual Stress

Over the last 30 years, there have been a growing number of applications that used portable XRD systems that use a small lightweight system to collect residual stress data on structures in the field. Demonstrable examples of this in the marine and military fields are the U.S. Navy's F-14 and P-3 aircraft, the U.S. Navy's Bob Hope class transport ship, and the Canadian Navy submarines [23], [24], [25]. These various systems used XRD to measure residual stress on a variety of metals including aluminum, steel, as well as nickel and chromium plating.

2. Naval Air Force

Brenner et al. completed a comprehensive study of residual stress on a number of naval aircraft systems determining if residual stress could be effectively measured, and then at what application this could be used for in practical Navy applications. This study looked at F-14 landing gear (stainless steel), P-3 propellers (aluminum), aircraft bearings and shafts (stainless steel), and nickel-plated coatings using a prototype portable Technology and Energy Corp (TEC) residual stress analysis machine. They were successful in measuring residual stress levels at the most common points of failure for each system [24]. The study had significant success in measuring residual stress and in finding risk of premature failure due to fatigue or stress corrosion cracking.

The study of the F-14 landing gear consisted of looking at 20 landing gear pistons with between 4 and 14 years of service life. XRD Measurements were taken along the base of the landing gear axle at four points along its circumference. Over the operational lifetime of these aircraft this area was known to be the most likely point of failure. Previous failures had come from fatigue, SCC, hydrogen embrittlement or a combination of these modes [24]. For any of these modes the presence of neutral or tensile residual stress conditions is an indicator that failure from one or a combination of these modes is

more likely. By taking these residual stress measurements, landing gear that showed surface tensile stresses could be either replaced or reworked.

The results of these measurements showed that while these measurements could determine risk of future failures the data was unable to show any useful insight into quantifying the current fatigue state of the piston. Figure (19) shows a comparison of all 80 data points taken shows no discernible pattern that would indicate a relation to the number of landings to the residual stresses on the pistons. This same lack of correlation for residual stress to current fatigue level was also observed in the other three aircraft components observed in this study [24].

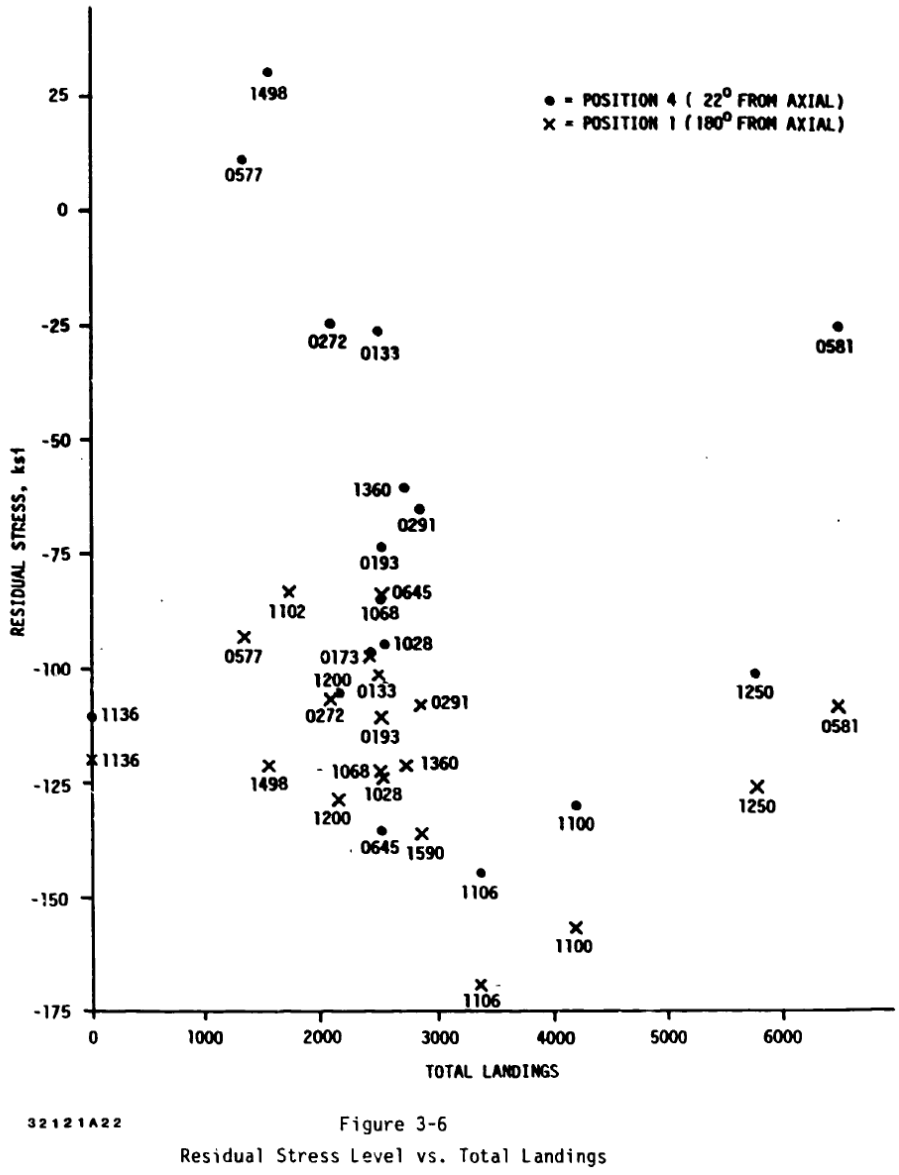

Figure 3-6
Residual Stress Level vs. Total Landings

Figure 19. Residual stress at most common failure point versus total landings. F-14 landing gear. From [24].

3. Canadian Victoria Class Submarine

Ferrell et al. completed a residual stress survey of an active Victoria class submarine looking at the main hoop welds holding the outer hull of the submarine together while it was in dry dock being repaired [25]. Using a Proto residual stress analyzer, they were able to complete a survey of the two main welds during a dry-

docking of the submarine. The pressure hull of a Victoria class submarine is made of HY80 stainless steel and is coated with a primer, adhesive and acoustic tiles. The primer and adhesive layer had to be chemically removed and the metal was electro polished 2 mm into the surface to avoid measuring the effects of surface deformations. This study measured residual stresses after a repair to a dent on the hull the affected hull plate was cut out and removed. Shown in Figure (20) is a complete profile of residual stresses after the repair to the hull was completed. Different parts of the structure showed major variations in residual stress due to the stress loading of structure after welding. The completed survey was used to make recommendations on the placement of strain gauges and in looking at the risk of crack propagation through the vessel's service life [25].

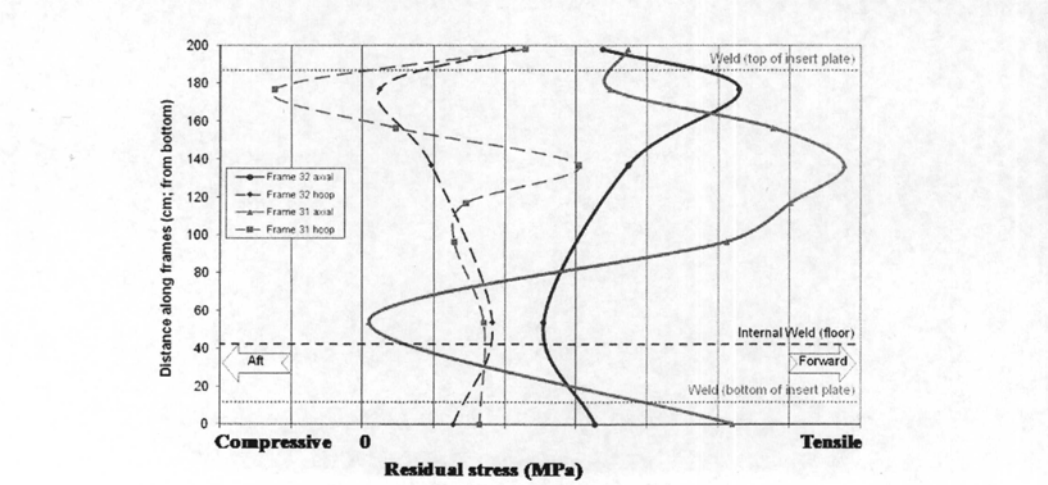

Figure 9. (Color online) Residential stress profiles (left) on frames welded to the pressure of submarine B (right). Dotted horizontal lines (left) depict the location of upper and lower plate welds.

Figure 20. Residual stress profile from Victoria Class submarine RCN. From [25].

4. USNS Bob Hope

U.S. Navy's SEALIFT command built seven roll-on roll-off transport ships, each of these vessels has approximately 14,000 cloverleaf tie down fittings. During initial runs and testing, over 400 cracks appeared from these fittings and failures occurred during operations at well below rated loads [23]. The massive extent of this problem

made the vessel operationally unusable unless a solution could be found. To address this problem, a root cause analysis board and investigation was held to find out the cause of these failures.

Testing of the affected welds quickly found that there was a region of excessively hard material around flame welded material. It was observed that the thermal shrinkage of the material was relatively high compared to the size of the cloverleaf. The use of the flame welding was chosen because of its speed and relatively low cost as the high deposition rate of the welding material allowed a single worker to complete this process with between 4 to 9 passes with the side effect of a relatively large weld nugget when compared to other possible welding techniques. To quantify this effect a portable XRD unit was employed to measure the effects of residual stress from the relatively large thermal shrinking around the cloverleafs. The XRD analysis showed residual stresses around the welds to be between +30 to 65 ksi. Close analysis of the micro structure of the cloverleaf's showed a layer of martensite the covered much of the surface of the cloverleafs. Within this layer, micro cracking was observed caused by the excessive tensile stresses from the welding. It was determined that the combination of a hard brittle surface layer combined with high tensile stresses was initiating cracking causing brittle failure at loads much lower than what was designed [23]. It was found that by changing the manufacturing process to remove the martensite, the cracking issues could be avoided. Subsequent XRD analysis found the revised residual stresses were reduced by an average of 32 ksi [23].

These examples of XRD use in the field clearly show significant utility for its use in determining quality and effectiveness of repair and manufacturing in the field and in conducting failure analysis. Knowing the effective residual stress after manufacturing and repair can give insight into the likely overall fatigue performance of the structure.

D. THESIS OBJECTIVES

This thesis assesses the feasibility of X-ray residual stress measurement techniques for use on board current naval structures and develops the requirements necessary for its applications on aluminum superstructures. Development of this

capability will primarily focus on measuring residual stress in 5000 series aluminum. The effects UIT peening processes on these measurements will be evaluated. Work will also conduct an analysis of potential problems and solutions for conducting these measurements on a U.S. Navy ship at dock.

1) Establish the feasibility of using portable X-ray diffractometers to measure residual stress in welded aluminum.

This will be done by collecting and analyzing baseline data provided by the manufacturers of portable XRD devices on materials used on current Navy surface ships. That data will be compared to each other and the advantages and disadvantages of the various equipment and methods will be discussed.

2) Assess the residual stress in 5456 aluminum caused by Ultra-sonic Impact Treatment (UIT).

Work will use laboratory X-ray residual stress on 5456 aluminum samples that are both UIT treated and untreated to characterize the residual stresses left by this process. This data will be compared with similar measurements on the same sample from a portable X-ray diffractometer.

3) Develop technical requirements for portable XRD for residual stress measurement on ship structures.

We will develop a comprehensive list of technical requirements for the portable XRD machine to be used in this project. Lists must include all physical and technical specifications for the X-ray diffractometer, as well as all the software and training need for data collection and analysis. Included will be the needed safety equipment with required interlocks for both field work and laboratory use.

4) Develop and analyze a case study for application of XRD residual stress to weld repairs on the superstructure of a Navy cruiser.

We will develop a problem statement coming from known issues on a current navy ship. We develop a detailed case study to look at the cause of the problem, and how portable XRD system will be operationally deployed and what relevant data will be taken, where it will be taken and what technical and safety issues must be addressed to complete this study.

III. OBJECTIVE #1: ESTABLISH THE FEASIBILITY OF USING XRD METHODS TO MEASURE RESIDUAL STRESS IN WELDED ALUMINUM

To determine the feasibly of measuring residual stress on active naval platforms, we obtained and examined results from three different organizations using different portable X-ray diffraction equipment on selected materials. In all cases, the goal was to measure residual stress as a function of distance from a metal-inert-gas (MIG) weld in a 5xxx alloy sample. While all three data sets demonstrate sensitivity to residual stress in these materials, important factors such as stress gradients, sample size, and grain size and texture are apparently important and must be addressed to ensure high-quality quantitative measurements. Lastly, this study will look at data taken at the Metal Improvement Company looking that will look at both residual stress versus distance from weld toe as well as residual stress versus depth on laser peen samples of AA5083-H116. To define whether these samples and results are feasible to use on an active marine platform, this study will look at the consistency, reliability and ability to account for the different material textures and surface effects.

A. METHODS

Two welded aluminum samples were used for these measurements. The first was a MIG welded plate of AA5083-H116. This first sample was made of ¼ inch thick rolled plate 36 X 24 inches [26]. The composition of this material is Mg 4.9%, Mn 1%, Cu 0.1%, Fe 0.4%, Si 0.4% Cr 0.25%, Ti 0.15% with the balance Al as certified by the American Bureau of shipping. This plate was cut in half parallel to the rolling direction of the plate material. These half sheets were then welded back together along the same line using metal inert gas (MIG) welding at Carderock Division, Naval Surface Warfare Center. Both sides of the material were clamped to the welding table during welding. Four welding passes were utilized, three on the top side and once along the root. Upon cooling all excess and slag was ground off of the plate surface. The welding procedure and specifications are shown in Table 3.

Table 3. Welding parameters for AA5083-H116 metal plate. From [26].

Pass	Volts	Wire Feed	Amps	Travel Speed	Weld Time	Inter-pass Temp	Remarks
1	23.9	273	121	17.4	1:16	69.6	Plate 1
2	25.1	336	136	17.4	1:15	118.3	
3	25.5	336	134	17.4	1:15	138	
4	25.1	336	138	17.4	1:14	72.9	Pass on the back of plate
1	23.7	273	122	17.4	1:15	69.8	Plate 2
2	25.4	336	134	17.4	1:15	120.8	
3	25.5	336	133	17.4	1:14	170.5	
4	24.9	336	139	17.4	1:16	72.3	Pass on the back of the plate

The second sample was cut from the forward section of bulkhead in a USN cruiser. The plate was made of AA5456-H116 and was ¼ inch thick on one side of the weld and was ½ inch thick on the other side of the weld. No other modifications were made to this plate other than removing the lagging. As this is a field sample, the exact welding conditions are not known, but by observation, the weld appeared to be a multi-pass MIG Figure (21).

Figure 21. (top) Laboratory welded aluminum (AA5083) sample (bottom) aluminum plate cut from USN cruiser (AA5456).

B. RESULTS FROM PROTO MANUFACTURING

Proto used a cobalt tube using Kα radiation at an accelerating voltage of 20 kV and a beam current of 4 mA using a 2mm aperture. Diffraction was measured from the {311} reflection at a 2θ angle of 148.9 degrees. To account for crystallographic texture in the sample, psi oscillations of 3 degrees were used. A series of d-spacings were measured using 11 psi tilts at plus and minus 0, 29, 22.48, 15.55, 10.28 and 2.4 degrees. The d-sin2psi analysis approach was used to calculate the strain and stress from each set of tilts. This measurement process was repeated at a series of locations moving transversely from the weld toe Figure (22).

Figure 22. Photograph showing measurement locations on AA 5456 cruiser plate.

Proto took data on residual stress in both the longitudinal and transverse directions at points from 0 to 10 mm away from the weld toe with a 2mm spacing on the control sample. Both sets of data show that stresses parallel to the weld were more tensile than the stresses in the transverse direction. This result is consistent with previous studies [14]. The importance of directional stress is also affected by the rolling direction of the material and can contribute to this stress gradient [27]. The data from Proto shows a moderate tensile stress within the first 10 mm from the weld toe. While this level of stress is generally low for residual stress near a gas weld on aluminum, this can be attributed to the carefully controlled conditions that the weld was made under. Also, the small length that the weld was cut into also would have relieved some of the residual stress Figure (23).

The result from taking the residual stress on the plate's surface from the toe weld to 20 mm was more surprising. The neutral to compressive stress state from the cruiser plate near the weld toe Figure (24) was not expected so close to a MIG weld. Normally, the residual stress from welding would leave a clearly tensile stress in this area. Further investigation showed that this result most likely came from compressive stresses caused by grinding off slag and spill from the weld surface. This grinding had the effect of peening the surface creating a small layer of compressed material at the surface.

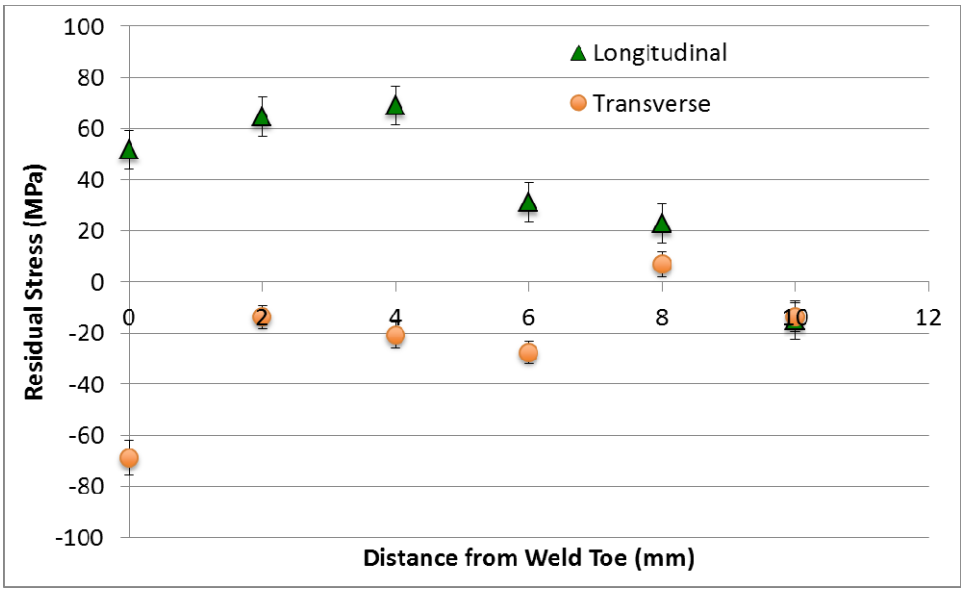

Figure 23. Data from AA5456 plate control weld. Residual stress versus distance from weld toe. Chart generated from data provided by Proto Manufacturing.

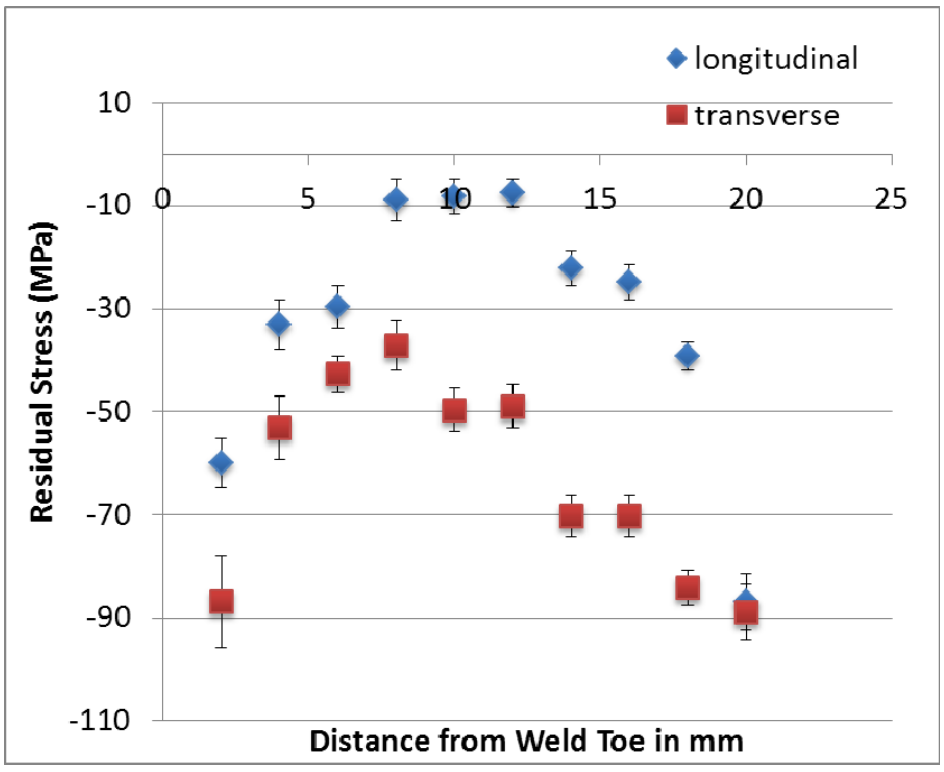

Figure 24. Plate #2: residual stress versus distance from weld toe in AA5083 plate from USN cruiser.

C. RESULTS FROM METALS IMPROVEMENT COMPANY USING A PROTO LXRD INSTRUMENT

Another set of measurements on the same MIG welded AA5083 plate were taken by B. Banazwski in collaboration with the Metal Improvement Company (MIC) using a Proto LXRD Non-Destructive residual stress measurement system Figure (26). This insrument has a MG200L goniometer that rotates the XRD goniometer in the ψ-direction. A separate mounting table was used to rotate the specimen in the ϕ-direction and the arm can easily be moved to repeat these steps in the x and y directions. Cobalt tubes and a 1mm beam width were used for all measurements at a power of 25 kV 20 mA. The {331} reflection was used due to make direct comparison between data from the portable Proto iXRD instrument and the laboratory model at MIC. This instrument used XRDWin 2.0 analysis software to do peak profile analysis and to compute d versus $\sin^2\psi$ analysis. Measurements were taken in directions both parallel and transverse to the direction of the weld to look at the directional stresses for comparison visual description is given in Figure (25).

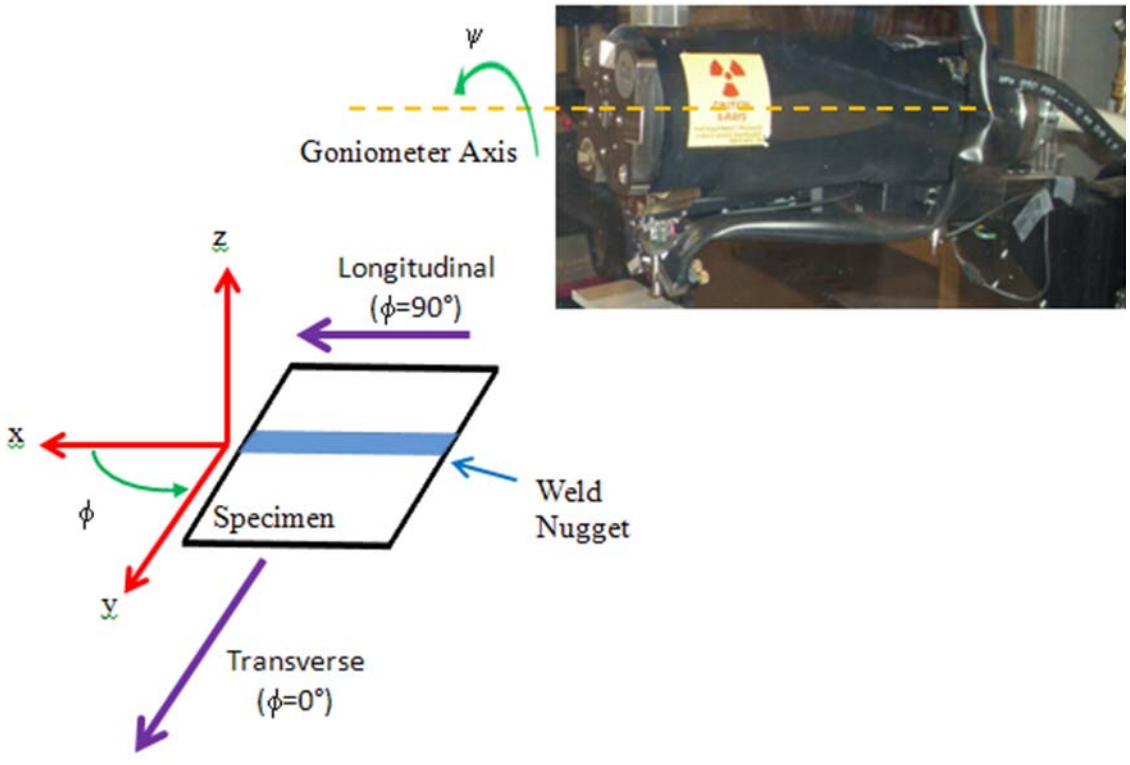

Figure 25. Proto XRD machine with description of coordinate system.

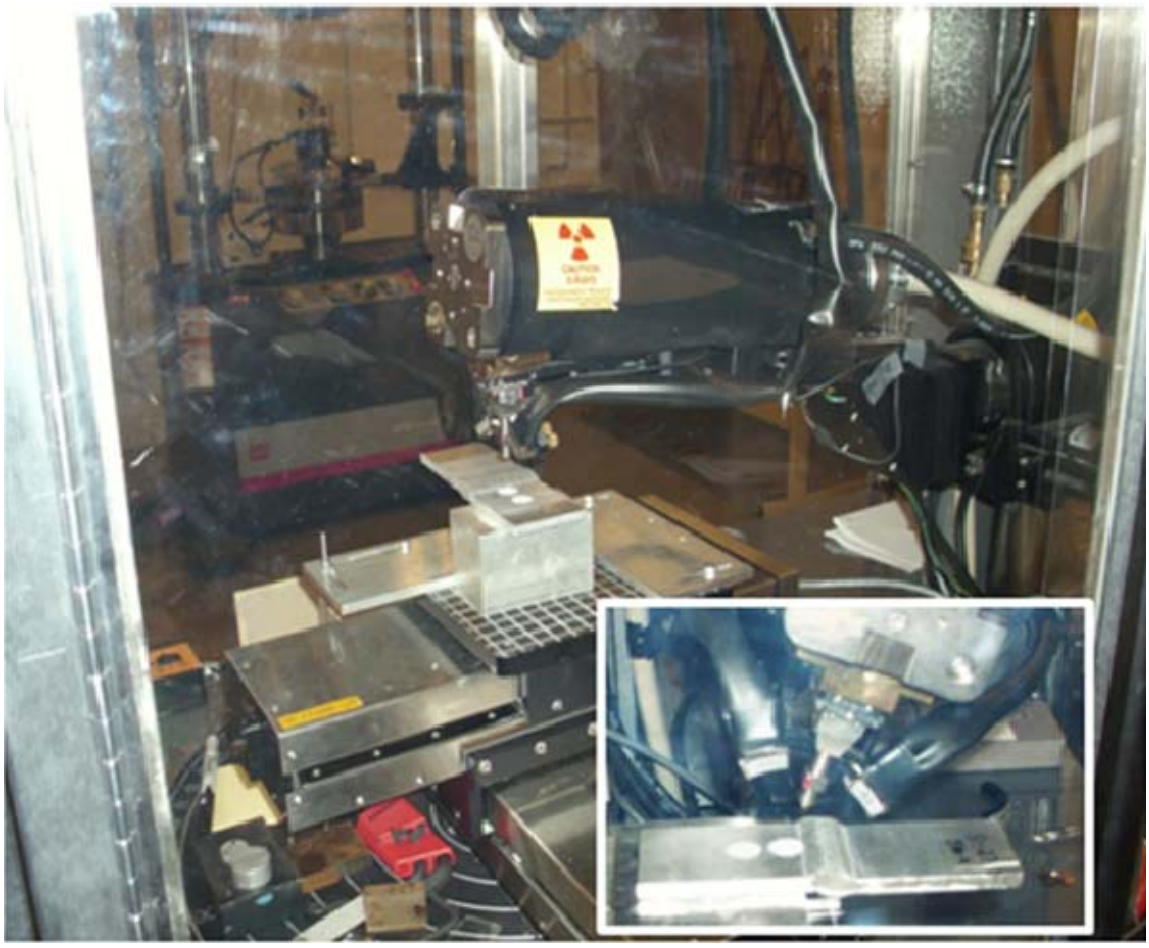

Figure 26. LXRD module measuring lab welded specimen. From [26].

The residual stresses versus observed from the control weld using the laboratory instrument at MIC tests were less tensile than what was seen at Proto Manufacturing Inc. The residual stress profiles away from the weld were similar in shape.. The relatively small tensile stresses show how effective the highly controlled welding process is effective at minimizing residual stress. The profile seen in the data Figure (27) does show the effect of the weld. A more compressive stress near the weld centerline quickly becomes more tensile, as it is measured in and around the heat affected zone, and then starts to drop off as the distance from the weld.

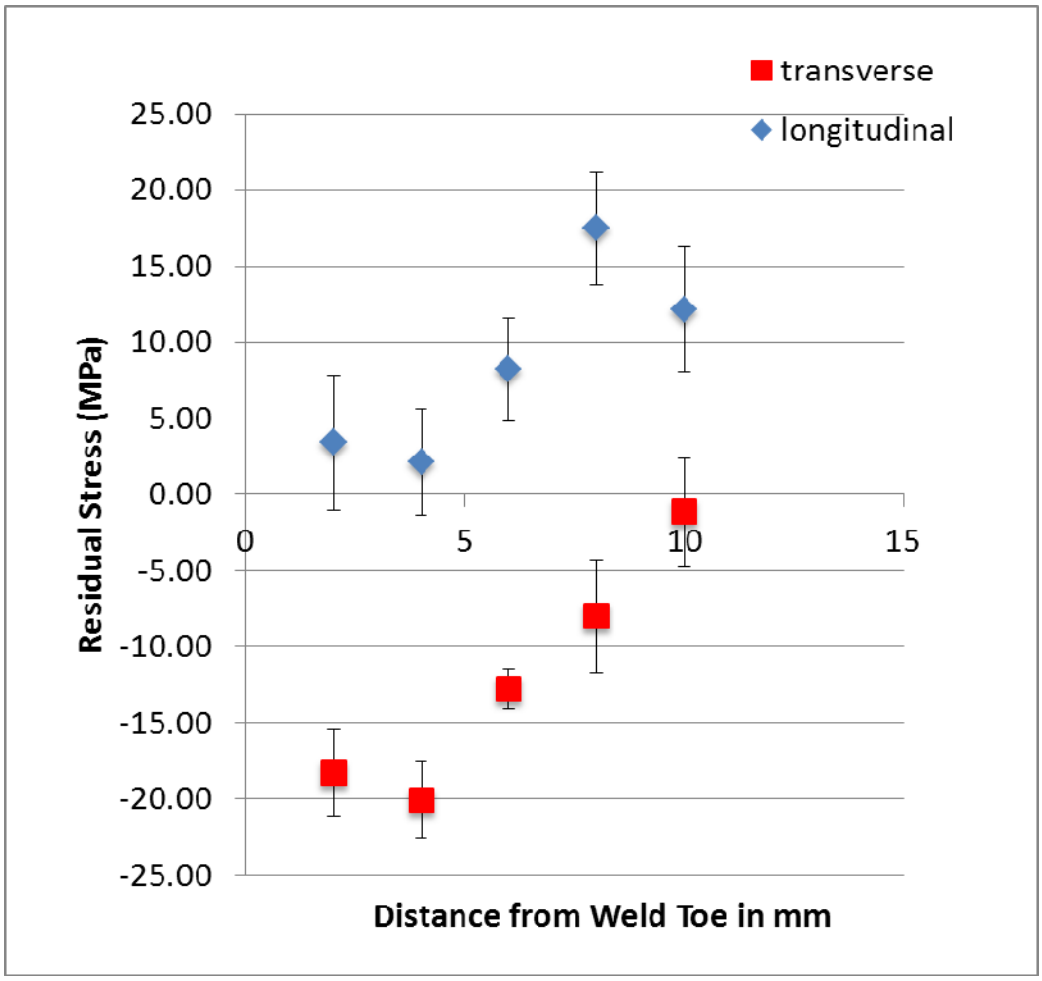

Figure 27. Control-weld residual stress versus distance from weld toe in AA5083 plate.

To examine the surface effects on the residual stress measurements, the sample was electro-polished and residual stress readings were taken at multiple points per depth.

Electro-polishing was used for two purposes, to remove surface stresses left over from grinding and to take variable measurements at different depths. The Metal Improvements Company used a Proto Electrolytic polisher Model 8818 to remove material to three different depths, 24.1, 254 and 508 micrometers. This polisher used a saltwater electrolyte comprised of 81 grams NaCl per liter of water with operating conditions of 85 volts and 70% max flow rate. The metal surface is first cleaned as impurities can vary the rate of reaction and create an uneven surface. The depth of removal of metal is described by a linear depth-time relationship that is dependent on the

voltage used. Table 4 shows this depth versus time relationship for 85 volts. Upon completion, the depth of each electro polished site was verified using a Mitutoyo deflector gauge, which has a precision of 2.54 micrometers [26]

Table 4. Electro polishing depth versus time at MIC.

Depth (μm)	Time (sec)
25.4	10
254	170
508	350

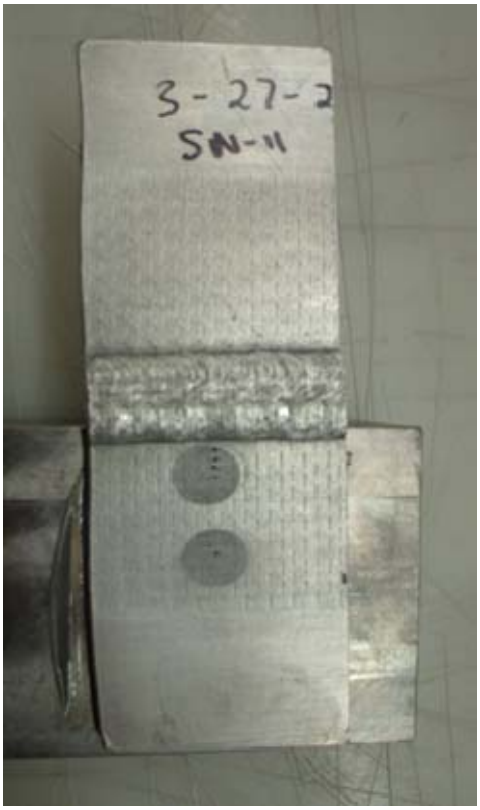

Figure 28. Electro polished sample peened in the laser peened condition. From [26].

A resulting residual stress versus depth profile taken at 6mm from the weld toe is shown in Figure (29). This plot shows a fairly consistent stress versus depth profile showing that at this spot the measurement stayed well within the margin of error for the measurement.

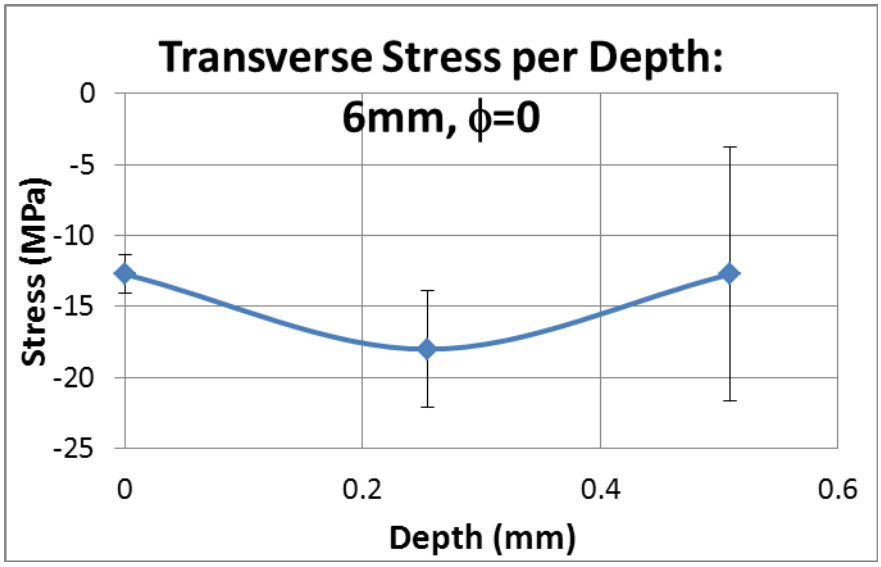

Figure 29. Residual stress versus depth for the control plate at 6mm from the weld toe. After [26].

D. RESIDUAL STRESS MEASUREMENTS FROM AMERICAN STRESS TECHNOLOGIES

American Stress Technologies used its XSTRESS 3000 portable instrument to demonstrate residual stress measurements with these same samples. AST took a set of residual stress measurements at depths from 0 to .68 mm into the metal at a distance of 1 inch from the weld centerline Figure (30). The XRD equipment used by AST was the XSTRESS 3000 G2/G2R X-ray stress analyzer Figure (31). The X3000 software analysis program also from AST was used to analyze the data. X-rays were generated with a Cr tube at 30 kV 10 mA with a 1 mm beam. Dual position sensitive detectors were employed in a modified symmetrical ψ geometry. Psi and phi oscillations at 0, 5, and 6 degrees were used to see what effect these oscillations would have in reducing noise in the data from any texture in the material.

Figure 30. Locations for measurements for depth profile on both samples.

Figure 31. AST XStress 3000 G2/G2R X-ray stress analyzer.

AST focused its measurements on the stress versus the depth after electro polishing. The electro polishing from 0 to .8 mm of depth subjects the measurements to differing textures of the material. The data was taken multiple times with both with and without psi oscillation of the X-ray beam to see if that can achieve better results. Figures (32 and 33) show the results with no tensile stresses above 40 MPa observed. The only large stresses noticed were on the surface of the field sample with a compressive stress of 80 MPa. This stress completely disappears at less than 0.1 mm of depth inside of the sample demonstrating again the importance of depth profiling in X-ray residual stress measurements. This data was taken about 10 mm from the toe weld. Both of these values are in the general range seen as those from MIC and Proto. The residual stress versus depth relationship remains fairly flat without the profile that the other companies showed. An important difference between the AST and the MIC and Proto tests was the use is of a chromium tube at AST versus the cobalt tube. Chromium X-rays do not penetrate as far into the metal as the X-rays from either copper or cobalt source would. The bars in the chart show the range of standard deviation and give a decent approximation of possible error in the data. While the overall results for the run using psi oscillation gives consistently lower stress values than the run without psi oscillation, in all but one case the data from the two different runs fit within each other's margin for error.

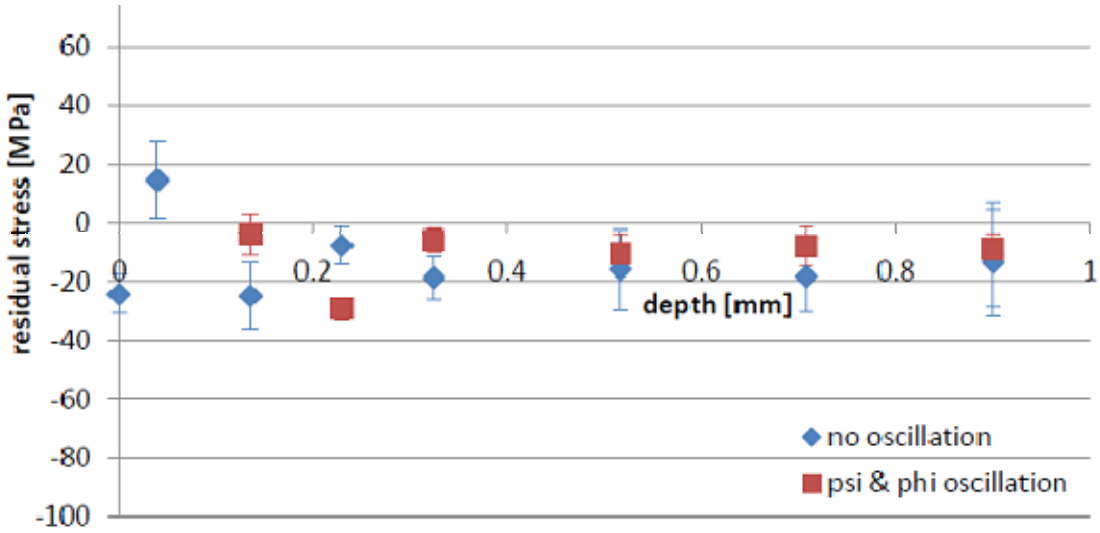

Figure 32. Residual stress versus depth control weld on AA5083 plate.

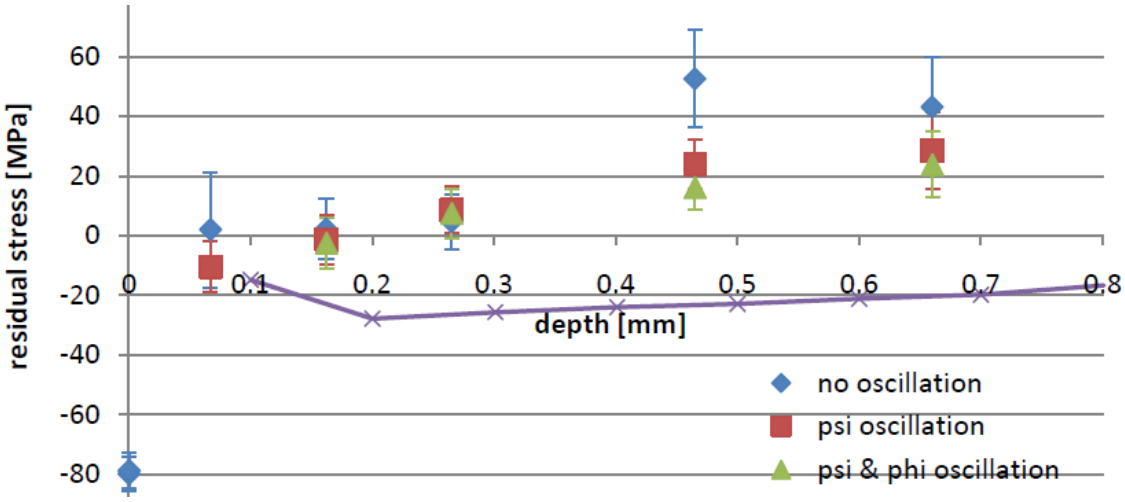

Figure 33. Residual stress versus depth (American Stress Technologies).

AST's study made was the use of both ψ and ϕ oscillations to reduce the effects of crystallographic texture. Data was taken both with no oscillation and then with ϕ plus or minus six degrees Figures (34 and 35). On the surface of the sample where there were significant issues with the texture of the material the d versus $\sin^2\psi$ plot is scattered and the data does provide a coherent result Figure (34). However, by adding in ϕoscillation the d. versus $\sin^2\psi$ while still not perfectly linear now provides a meaningful result. This does show that using this technique can be effective and reducing the effects of texture. However, to some degree, this experiment is offset by the fact that MST and Proto have shown ability to get significantly better data without this method by using either copper or cobalt radiation.

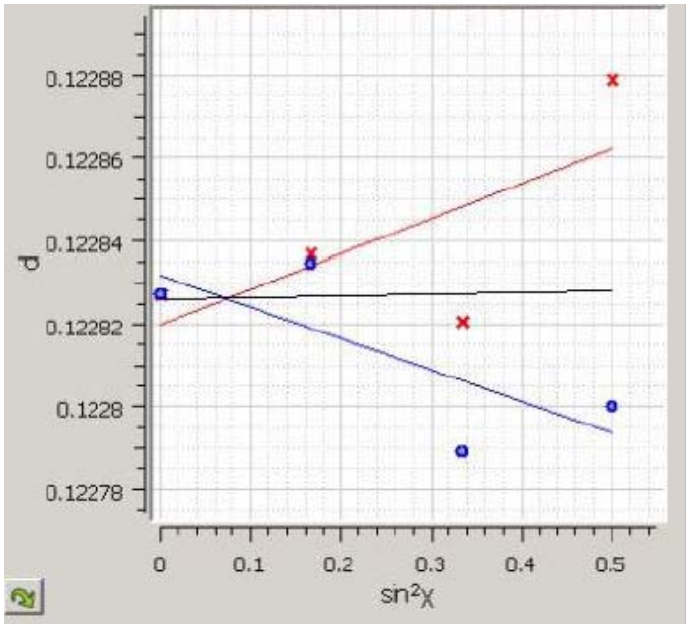

Figure 34. d versus $\sin^2\psi$without ϕ oscillation. Red values are -ψ angles, blue is +$\tilde{\psi}$.

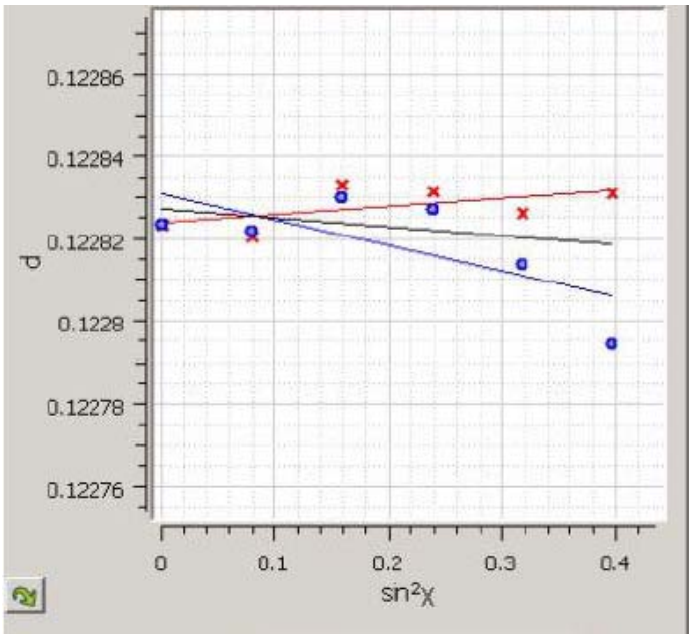

Figure 35. d versus $\sin^2\psi$ with ϕ oscillation. Red values are -ψangles, blue is +$\tilde{\psi}$.

E. FEASIBILITY

Looking at these results, it is clear that using XRD residual stress techniques can be an invaluable tool in understanding the stress state of a structure both in laboratory

samples and in field sampling. Multiple companies and universities have successfully used this technique to demonstrate better understanding of aluminum specimens of a variety of different compositions and uses. However, the clear lack of consistency in this data show that developing and maintaining a working methodology and careful analysis and use of the data provided by this technique of high difficulty and crucial importance.

Minor effects from very subtle causes as surface deformation, grain texture, vibration, and anisotropy of the metal and tube choice can all significantly alter the results. To effectively use this method in the field and gain reasonable results, careful methodology and data analysis techniques must be developed and utilized.

To get useable results from XRD residual stress measurements, a number of major causes of very significant error must be mitigated. The first of these errors is the effect of surface effects. Figure (33) clearly shows a large change in residual stress in the first .1 mm of the sample. In this case, it is likely that grinding off slag after welding and other physical peening effects occurred. To mitigate error from surface effects, electro polishing and taking samples from at least .1 mm below the surface are needed?

The second major source of error is the somewhat unpredictable affect that both texture and the anisotropy of the metal have on residual stress measurements. This can be seen in oscillatory patterns in the $\sin^2\psi$ plots. There are three ways that this can be mitigated: by using oscillations in the phi direction, such as AST did in Figures (32 and 33), by taking data using the {400} or {333} reflections, which are less sensitive to texture effects; or by taking a full tensor measurement. Unfortunately, the {400} and {333} reflections in aluminum often fall outside the range of most X-ray diffractometers. The best way to get accurate results in this situation is to use a full tensor analysis; however, as residual stress measurements are a time intensive procedure completing the additional measurements required to a full tensor analysis may be impractical.

XRD residual stress data is an excellent method for understanding the direction and magnitude of residual stress in a metal. Applied to naval structures, this information

can be used to understand a naval structures risk of failure from fatigue, stress corrosion cracking, and give real feedback on the quality and damage induced by repairing or altering the structure of the vessel.

IV. OBJECTIVE #2: MEASURE RESIDUAL STRESSES CAUSED BY ULTRASONIC IMPACT TREATMENT ON ALUMINUM ALLOY 5456 USING X-RAY DIFFRACTION.

This section discusses the use of X-ray diffraction to measure residual stresses generated by ultrasonic impact treatment (UIT) on coupons of aluminum alloy 5456. This section describes experiments performed at the Naval Postgraduate School (NPS) using laboratory X-ray diffraction and compares them with data taken using a portable X-ray diffractometer from Technology for Energy Corporation (TEC).

A. METHOD

This set of experiments examined residual stresses taken from a Navy cruiser. Four samples of aluminum alloy 5456 aluminum were taken from two different locations on the superstructure of a Navy cruiser. UIT was performed at these locations to intentionally impart compressive residual stress, which should help to mitigate stress corrosion cracking and allow successful weld repairs. Samples 2cm x 2cm in dimension were taken from each location before and after the UIT treatment was applied.

Residual stress measurements using a portable X-ray diffractometer were performed on these extracted samples by Technology for Energy Corporation (TEC). TEC used the TEC 4000 X-ray diffraction system using a proportional counter detector with a power of 30 kV and 6.7 mA. The X-rays were generated using a copper tube with a vanadium filter for Kβ suppression. The readings were taken from the diffraction using the {511/333} peaks. The use of these peaks gives a better strain resolution due to the high diffraction angle around 160 degrees in 2θ,. as well as deeper penetration than Cr radiation. The instrument was calibrated with a standard powdered aluminum sample. TEC took residual stress measurements starting from the surface to a final depth of .254 mm using electro polishing to remove material from the surface.

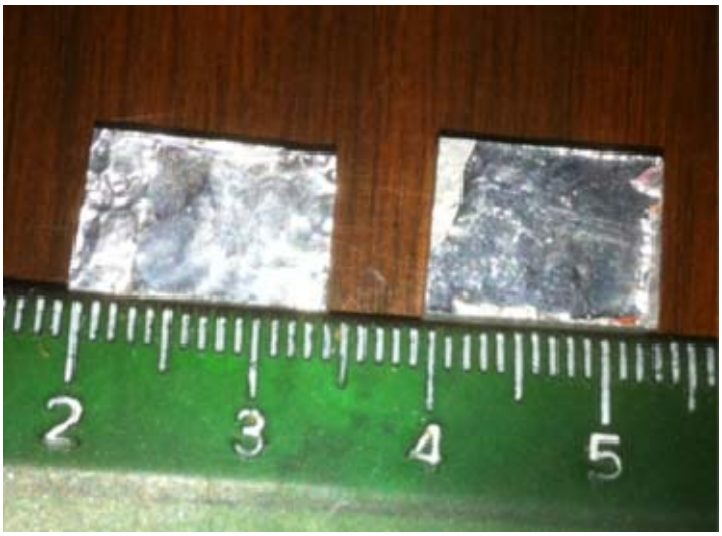

Figure 36. Electro polished aluminum samples taken from Navy cruiser. Left sample has been UIT treated. Ruler in picture is in centimeters.

The residual stress measurements using x–ray diffraction were repeated at NPS. The measurements were repeated for two reasons: 1.) to gain experience in the X-ray diffraction residual stress measurement at NPS and 2.) To assess any differences between residual stresses measured by a laboratory diffractometer compared with data from a portable diffractometer. The measurements taken at NPS were taken after sample was electro polished at TEC and without any further material removal or polishing. The residual surface deformation from the UIT process was still visible on the treated sample Figure (37). The residual stress measurements were taken on a Philips analytical X-ray diffractometer (model PW 1830) using a copper tube at a power of 35 kV and 30 mA. X-rays were set up to strike the middle of sample at an omega angle of 69 degrees to gain the needed refection intensity. The machine ran 2θ values from 113.5 to 177.5 degrees at intervals of .02 degrees with a dwell time of 2 seconds. Residual stress measurements are taken on the solid sample detector on the left in Figure (36). The samples were secured on the machine with an epoxy, and the sample height was set by raising the sample until physical contact was made with an alignment pin in the center of the goniometer circle.

Figure 37. NPS XRD machine. Residual stress detector on the left.

Measurements of the residual stress were collected using the d-sin$^2\psi$ method. The readings were taken on the {420} peak at approximately 115 degrees. The use of the {420} peak was due to limitations of the equipment. The {422} or {333} peak would be preferable for measuring residual stress as their higher peak angles give better resolution from the d spacing [11]. A total of seven measurements were taken on each sample using ψangles of 0, 16.8, 24.1, 30, 35.3, 40.2 and 45

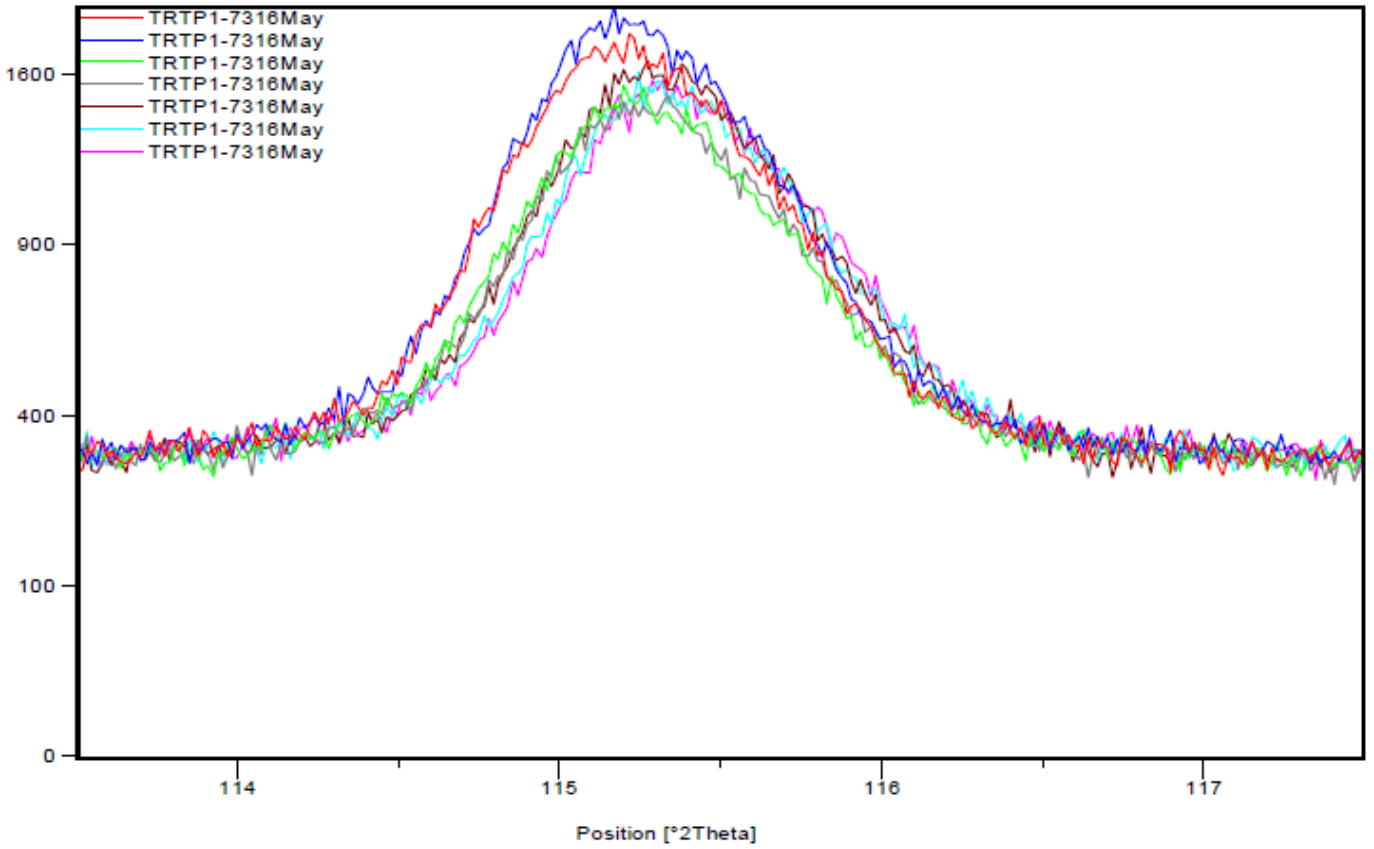

Figure 38. XRD peaks from plate #1.

B. DATA ANALYSIS

A multi-step, data reduction method was used to extract the residual strain from the measured diffraction profiles. The data reduction involved several steps including: removal of background, peak identification, removal of kα-2 peak, and peak profile fitting. These data reduction procedures were performed using the commercial Philips Xpert Highscore software. Each diffraction peak was analyzed individually and a background value was calculated, shown in the green line in Figure (40). The copper X-ray radiation has second peak called K$\tilde{\alpha}$-2 that so close to the K$\tilde{\alpha}$-1 peak that above in Figure (39) it looks like one peak. Since the wavelengths of both of these peaks are known, the analysis program is able to strip out the part of the peak caused by Kα–2 mathematically, which gives the peak shown in Figure (40). With the Kα–1 peak determined the software makes a guess as to where the center of the peak is then applies a data fitting algorithm that finds the statistical center. The quality of the peak fitting is shown in the residual plot, which is the difference plot between the experimental signal and the peak fit calculated using this procedure Figure (41). A flat, low-amplitude residual is indicative of a high quality peak fit. The peak centroid for each peak was converted into a d-spacing for the {420} reflection using Bragg's law Equation (6). The result of this data reduction was a set of d-spacing's as a function of ψ angle for the {420} reflection.

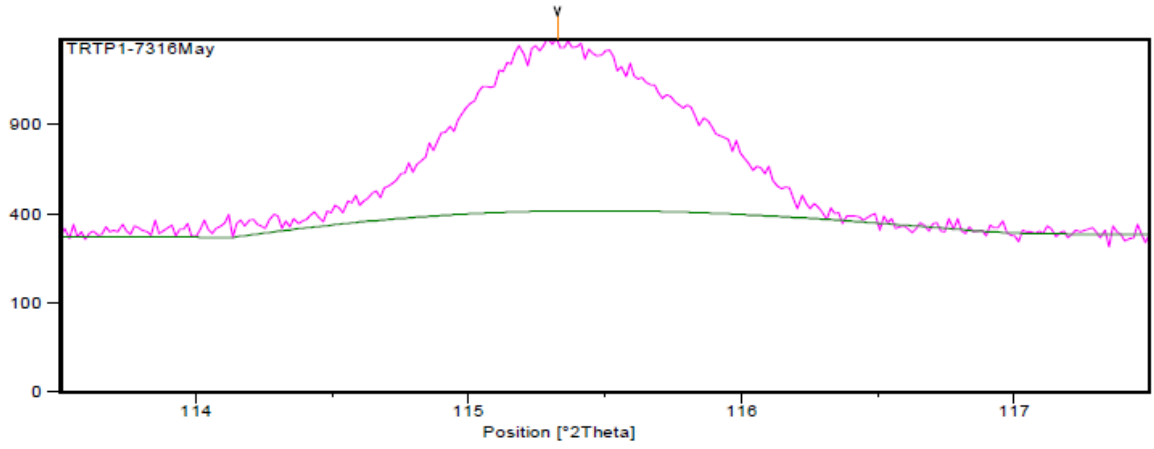

Figure 39. XRD peak for sample from Plate #1.

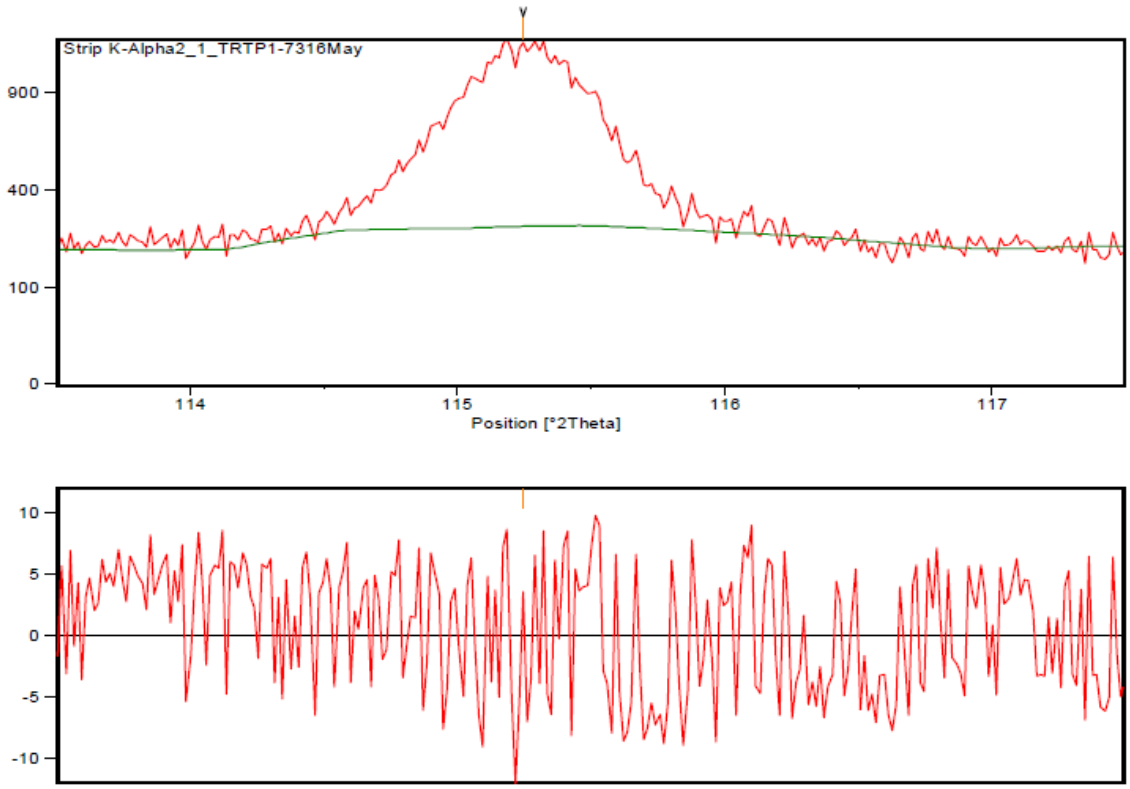

Figure 40. Data from Figure (39) with K alpha 2 stripped with fitting plot below.

"d versus $\sin^2\psi$" Technique

The residual strains and stresses were calculated from the data in Figure (39) using the d versus $\sin^2\psi$ technique. This method simplifies the determination of strain and stress by making two assumptions about the nature of the stress being measured. The assumptions are that the strain is two dimensional in nature and that there is no stress in the z direction. As residual stresses being measured are caused by the restriction with a metal plate, the degree of stress that is being applied in the z direction should be minimal and therefore the residual stress is biaxial [20]. Using this assumption, the full stress tensor simplifies into Equation (16). This simplified equation describes a linear relationship between the measured d spacing and $\sin^2\tilde{\psi}$.

$$\frac{d_{\phi\psi} - d_0}{d_0} = \frac{1+\nu}{E}\sigma_\phi \sin^2\psi - \frac{\nu}{E}(\sigma_{11} - \sigma_{22}) \tag{16}$$

The XRD analysis gives the change in d spacing as compared to a d_0. This value is normally not known but can be replaced by taking the d spacing at $\psi = 0$. Young's modulus (E) and Poisson's ratio (v) and known constants of the material this leaves only σ_ϕ, σ_{11} and σ_{22} as unknowns. σ_ϕ is found by taking the slope of the d versus $\sin^2\psi$ plot. With this information the principal stresses can be calculated. The total error introduced by this method is less than .1% of the stress value and is significantly smaller than the other error factors in this method [20].

Not all d versus $\sin^2\psi$ behavior is the same. If linear or branched behavior, as seen in parts "a" and "b" in Figure (41), the stress equation is valid and very closely predicts the behavior of the system. The branching seen in Figure (41b) is caused by the out of plane stresses being unequal to zero. For the cases in both a and b, a linear least squares fit will give determine the residual stress for that reading. Note, that the positive slope of the least squares line is positive; this will indicate a tensile stress and if negative a compressive stress. If there is significant oscillation in the plot, as seen in Figure (40c), then the system is behaving in a manner that d versus $\sin^2\psi$ plot cannot predict.

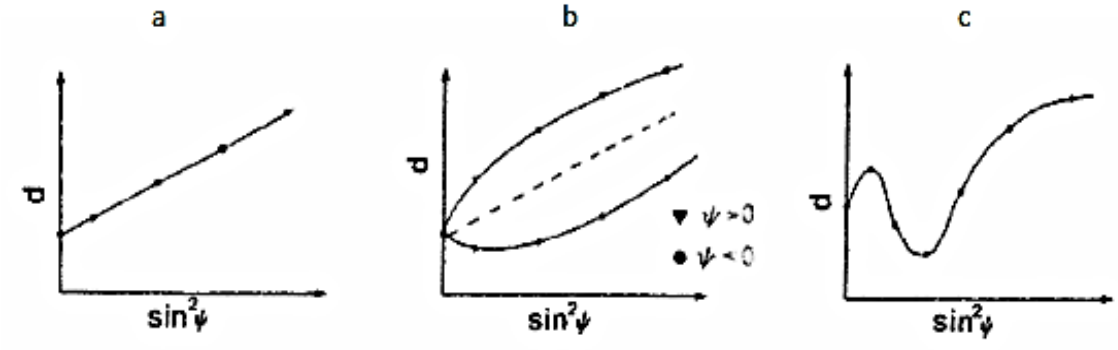

Figure 41. (a) regular linear behavior, (b) branched behavior, (c) oscillatory behavior. From [20]

The d versus $\sin^2\psi$ plots for the UIT treated samples were relatively linear giving very clean data. This is contrast to the oscillatory behavior seen in the high stress control sample shown in Figure (44). This is most likely caused by the way that the grain structure of the metal is refined by the UIT process. The random deformation caused by

the hammer repeatedly striking the surface leaves a very consistent stress that is nearly truly biaxial. This has significant implications in the practical field measurements of UIT treated samples in that the d versus $\sin^2\psi$ method can be confidently used. This method can be effective with few measurements and save a very significant amount of time compared to using the full tensor measurements.

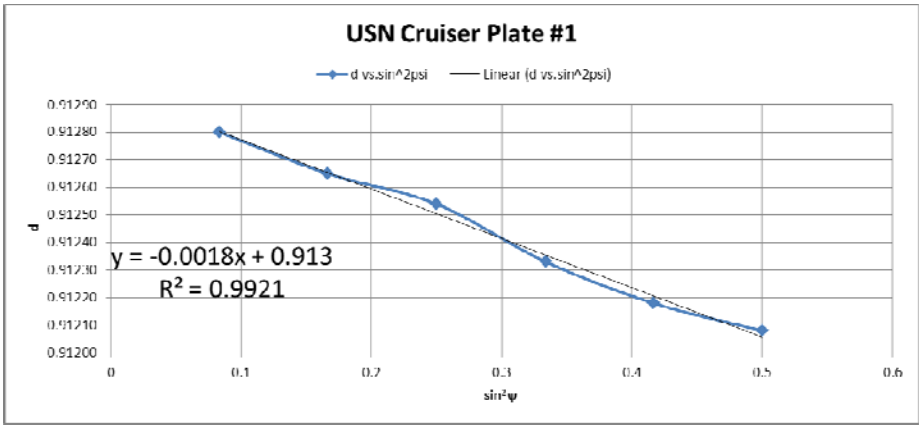

Figure 42. d versus $\sin^2\psi$ plot for Plate #1 from the Navy cruiser UIT treated sample.

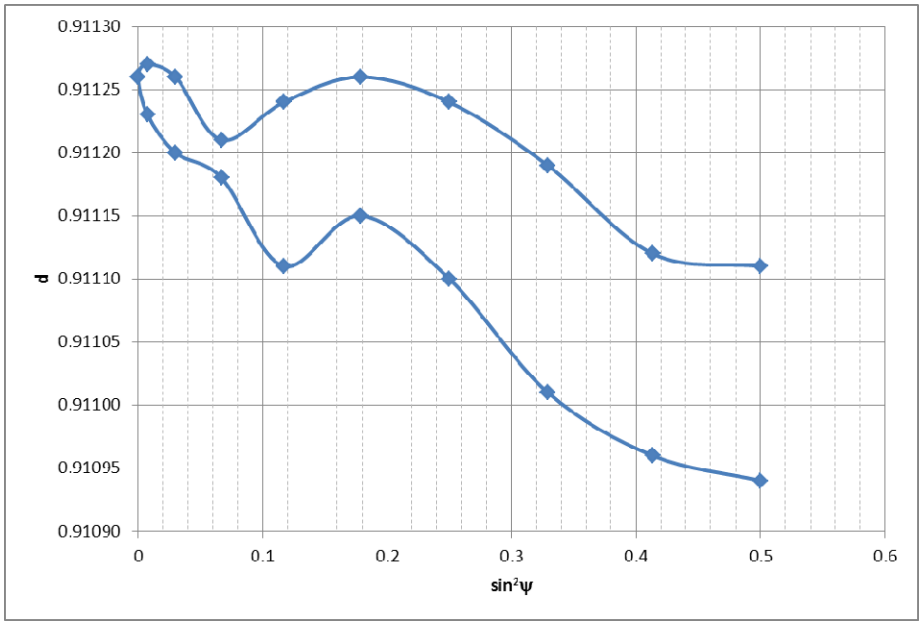

Figure 43. d versus. $\sin^2\psi$ plot for a high stress control sample.

To calculate out the final residual stress from the above plots, the strain values were calculated by calculating the d spacing at each measured ψ angle. With the d spacing known, the difference between the d spacing's at each angle can be calculated into a strain value e33 Figure (44). By plotting this strain value versus $\sin^2\psi$, the slope of this line can be used as σ_ϕ, and then the residual stress can be calculated.

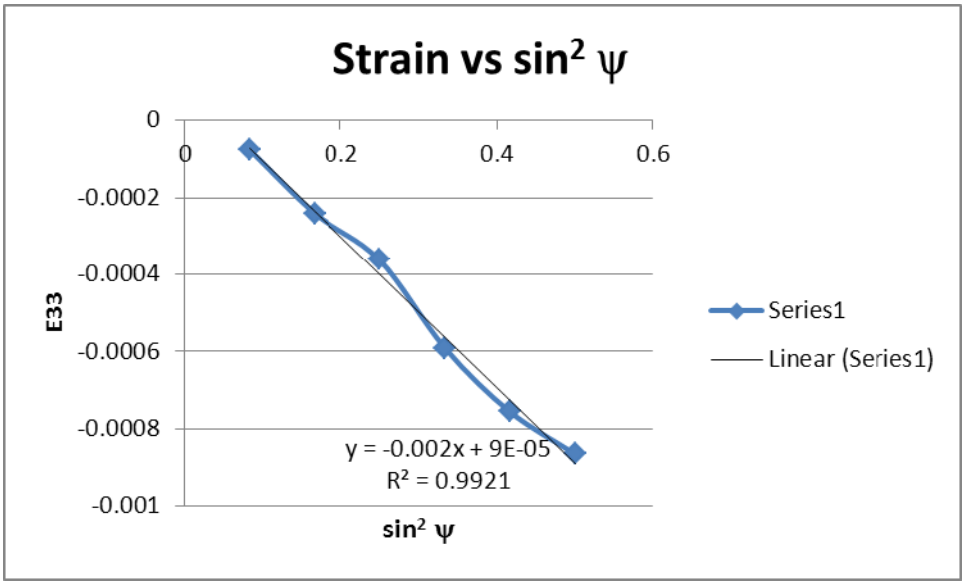

Figure 44. Strain versus. $\sin^2\psi$.

C. RESULTS

The data from the residual stress test at NPS came out fairly close to what was done at TEC Table (3). Three of the four measurements came out to within 20 MPa of each other, which is within a reasonable margin of error for this kind of measurement. Treated Plate #1 was significantly lower than the TEC result by 40 MPa. Possible sources of this error may be from texture issues and also due to the fact that different diffraction peaks were measured the {420} at NPS versus the {511/333} at TEC. In this case, the {511/333} peaks are the more likely and accurate choice as higher 2θ angles generally lead to better resolution [11]. In this case, two very different X-ray diffraction machines

developed comparable and useable results for the same samples. The consistent and linear d versus $\sin^2\psi$ plots shows that this feasible and practical to use for measuring residual stress on UIT specimens.

Table 5. Residual stress of USN Cruiser at .254mm depth. Comparing results from NPS and TEC.

	NPS (MPa)	TEC (MPa)
Untreated Plate #1	-79	-71.1
Treated Plate #1	-106	-146
Untreated Plate #2	-85	-91.7
Treated Plate #2	-127	-110

TEC also completed a depth profile of these same samples taking measurements of each sample at 6 different depths Figures (43 and 44). The smooth and shallow playground slide shape of the curve to depth is a very good result and fits with expected residual stresses in a plate. The consistent curve shows a lack of noise in the results and helps gain confidence in the data. The relatively small increase in stress just below the surface layer is much lower for this sample than for data taken from other compressive stress additive techniques. Other techniques, such as laser peening or shot peening, have much more variation in measured surface stress [19]. If electro polishing is not a practical option, the surface of an unblemished UIT plate can give a reasonable estimate as to the overall stress characteristics of the plate.

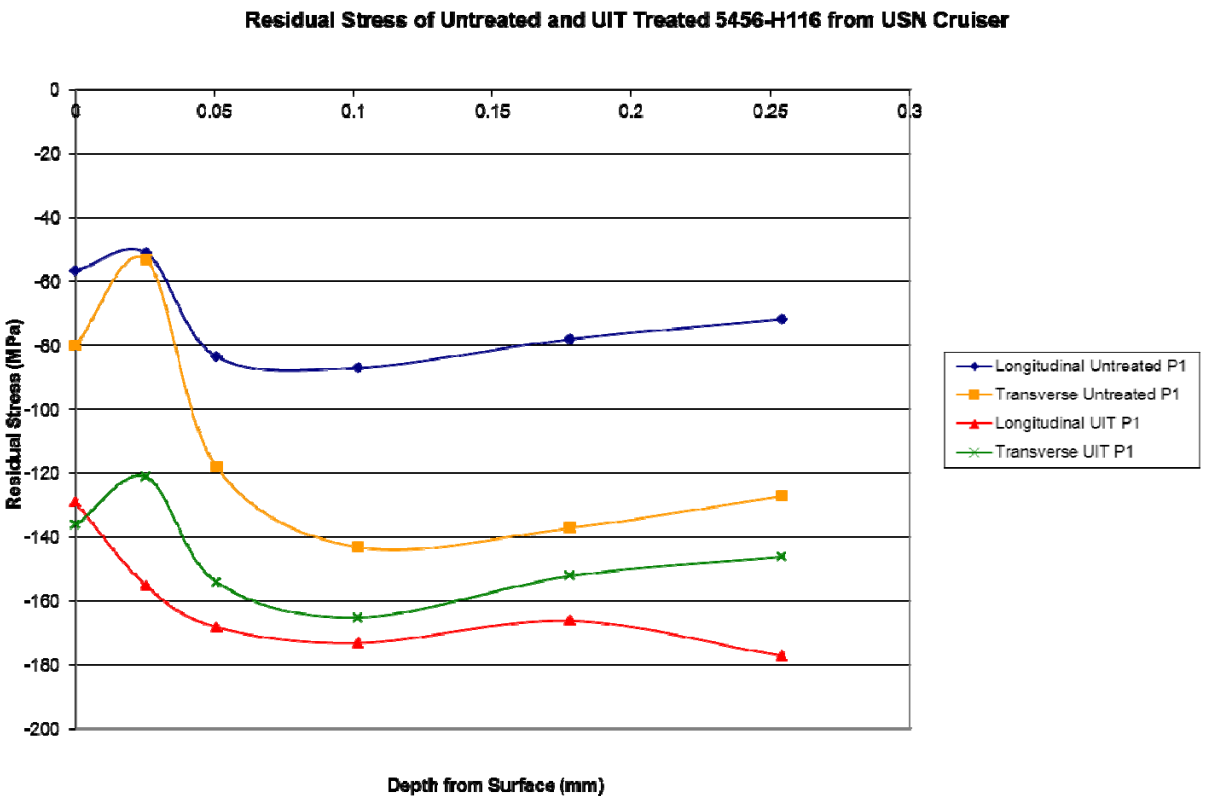

Figure 45. Plate #1 residual stress versus depth. Four linear series data courtesy of TEC.

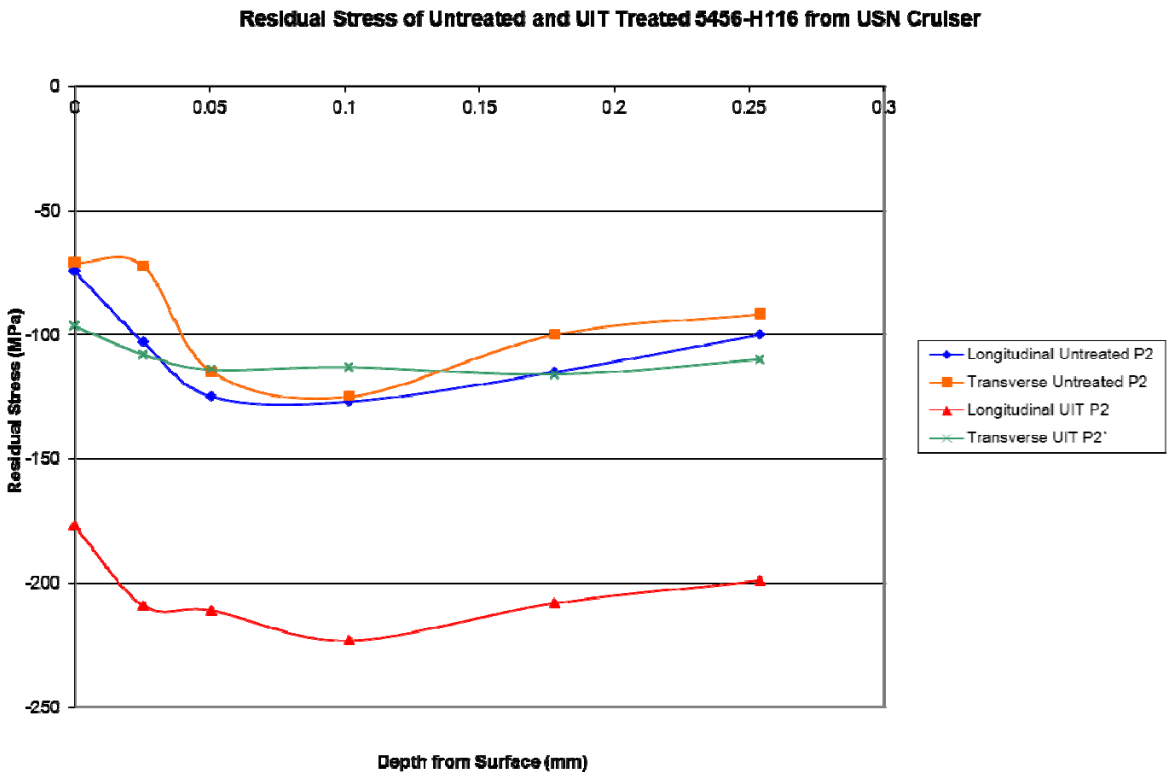

Figure 46. Plate #2 residual stress versus depth. Linear data series courtesy of TEC.

Overall, the use of XRD residual stress measurements on UIT samples is very practical and is in fact from the perspective of measurement easier than performing the same measurements on untreated or laser peened samples. The randomness of the method and the grain refinement that occurs due to UIT treatment creates an ideal environment for these measurements Figure (47).

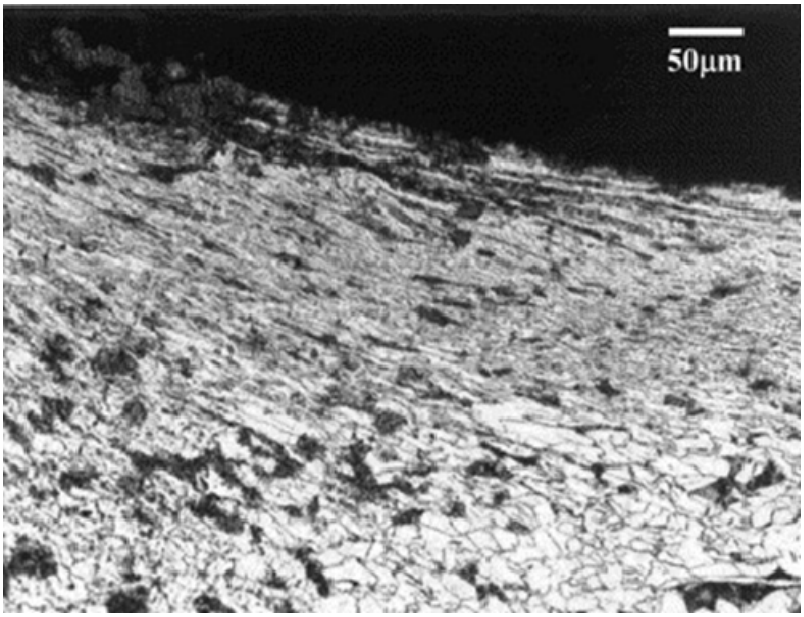

Figure 47. Micrograph showing layer of grain refinement due to UIT treatment in A588-97B steel [28].

THIS PAGE INTENTIONALLY LEFT BLANK

V. OBJECTIVE #3: DEVELOP TECHNICAL REQUIREMENTS FOR PORTABLE XRD FOR RESIDUAL STRESS MEASUREMENT ON SHIP STRUCTURES

In order to complete the purchase and develop full operating and safety procedures for its use, a full requirements document must be created to lay out the specific technical specifications that this system must meet in order to complete the desired long term research goals in measuring and studying stress on aluminum shipboard structures. The stated goal of the document is to a set of specific, tangible machine and software specifications for a XRD device that will be portable, capable of taking and analyzing residual stress measurements on aluminum and steel maritime platforms while either tied to the pier or in dry-dock status. This device will be easily mobile and able to take readings at one point at a time on either the hull or the superstructure of any navy surface ship.

A. METHOD

Market research was conducted identifying what companies manufacture portable XRD devices for residual stress measurements. Three U.S.-based companies were identified as selling instruments that would take residual stress measurements using a portable device. These companies were Proto Manufacturing Figure (48), American Stress Technologies (AST) Figure (49) and TEC Figure (50). Each of these companies was asked for detailed technical specifications and a budgetary estimate for their particular instrument. After reviewing the technical specifications from each of the companies and reviewing literature from previous uses of XRD residual stress measurements, a group consisting of one research professor and military research students brainstormed requirements. The requirements were set up in two different lists: 1.) what was required from the X-ray producing instrument to gather accurate and reliable data from the maritime structure, and 2.) particular attributes that are needed to successfully make these measurements on board a ship—Table 6.

Table 6. Comparison of Proto, AST and TEC key specifications.

	Proto	AST	TEC
Tubes	Mn, Cr, Co, Cu	Mn, Cr, Co, Cu	Cu, Fe, Mn, V, Ti, Co
Data collection	Laptop/inbuilt program	Laptop/inbuilt program	Laptop/in-built program
Electro polisher	Electrolyte A	Salt water	Salt water
Alignment	Measuring kit	not specified	Automatic Z alignment
Psi arc	180 degrees	-45 to 45 degrees in steps	-45 to 60 degrees
x and y axis	225 mm travel in x and y	N/A	N/A
Psi oscillation	Full range of motion	+ or - 6 degrees	No range limit
Omega arc	N/A	180 degrees	N/A
2 Theta range	18 or 30 degree range	39 degrees	50 degree range
Placement	Stand with magnetic feet	Magnetic anchoring tripod legs	Stand with magnetic feet
Shutter specs	.5, 1 and 2 mm	1, 2, 3, 4, 5 mm	0.5, 1.0, 1.5, 2.0, 3.0 X 5.0 mm
Automation	Fully automatic	Psi and 2 Theta directions	Psi and 2 Theta directions
Training	At Proto facility	On location	On site, or at TEC facility
Cooling	Recirculating	Recirculating	Recirculating

Figure 48. AST portable XRD system.

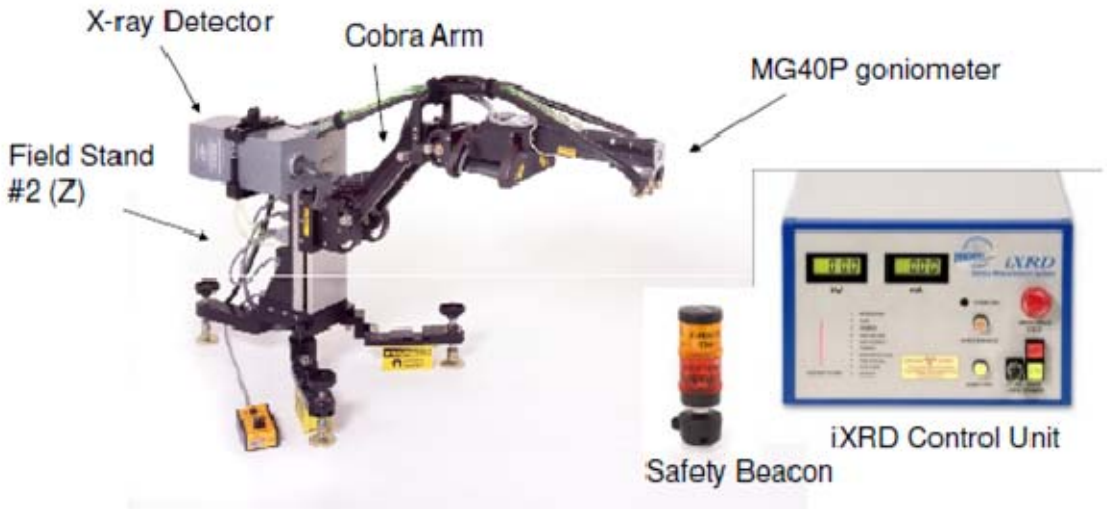

Figure 49. Proto XRD system.

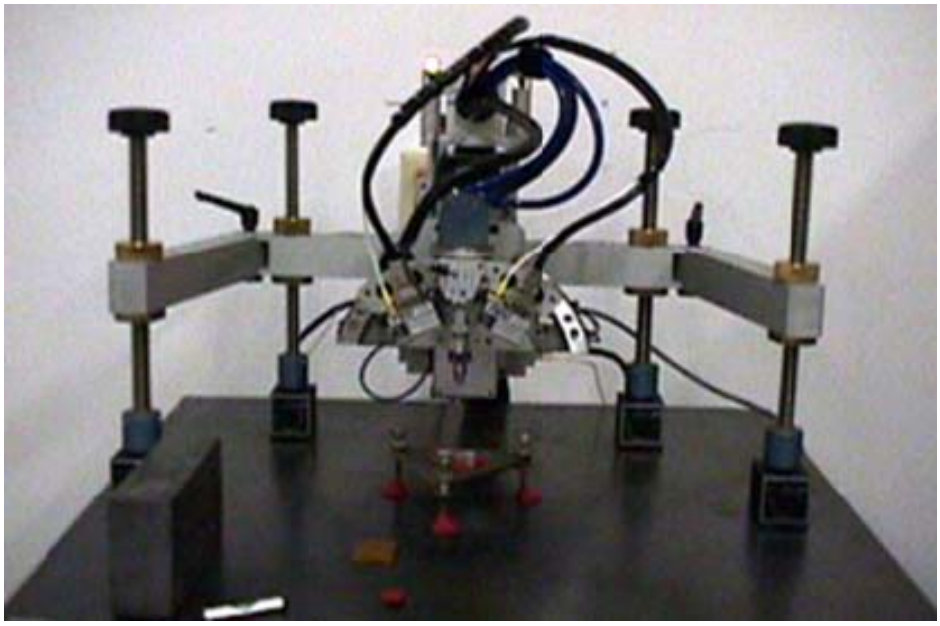

Figure 50. TEC portable XRD system.

B. KEY CHALLENGES

Several challenges were identified early on that needed specific focus. The first of these was radiation safety. Current XRD use at the Naval Postgraduate School is confined to a set room with limited key access and the XRD machine is housed in a

radiation safety enclosure, surrounded by an X-ray absorbing materials on all sides. When utilizing this method in the field, portable X-ray shielding must be used, and its use must be qualified by Navy radiation safety personnel.

To estimate the radiation safety risks involved in using a portable X-ray diffractometer, the percent transmission of common XRD radiation wavelengths was calculated in relevant materials and air. This can be simply calculated as shown in Equation (17) .

- $I = I_0 e^{-\left(\frac{\mu}{\rho}\right)x}$ (17)

Where μ is the mass attenuation coefficient as found in a chart [11] and ρis the density of the material. With this equation penetration, values I_O /I were calculated for aluminum, iron, polycarbonate and air using Co, Cu and Cr X-ray tubes. Max Exposure was taken by calculating radiation intensity of an unshielded X-ray tube at 35 kV and 30 mA power. These conditions gave very conservative estimates on possible exposure as all of the portable systems being looked at operate and much lower power. These calculations also assumed that there no shielding was present, just X-ray emission from a bare X-ray tube. In reality, all portable diffratcometers use a small (1 mm) aperture to confine the X-ray beam, thus only a fraction of this radiation will leave the device. The results in Table 7 show that less than .1% of X-rays will penetrate through more than .09 cm of aluminum, more than .02 cm of iron, more than 2 cm of plastic, or more than 10 meters of air. A board a naval ship, the aluminum or steel compartments will be adequate to contain any X-rays produced in making residual stress measurements. Safety curtains can also be placed to block the X-rays from reaching the operator. With these basic safety precautions, an acceptable safety plan can be enacted to meet all federal and military radiation safety standards.

The second major challenge comes from using a portable XRD system on a vertical surface. All current systems are designed to work on horizontal surfaces. A vertical surface (e.g., a bulkhead) requires mounting of the instrument on the bulkhead. All three of portable come with magnetic feet as a solution to this situation. However, as the focus of this research is on aluminum, a second solution is needed. Two solutions that

have been discussed in depth were to use suction cups instead of magnets. The second solution is to simply loft the machine into position using a separate platform. Both of these solutions were deemed acceptable but somewhat problematic. Placing the XRD system on an elevated platform makes it difficult to keep an accurate distance between the X-ray gun and the aluminum surface. Suction cups may require separate surface treatments to ensure a secure fixture to the surface. The machine from Proto Figure (49) is particularly well suited to placing it on a separate platform as the robot arm has a complete range of motion allowing the machine to set horizontally on a lifting platform while still taking readings on a vertical surface.

Automation was the next major issue that was discussed. Readings need to be taken about the 2 Theta, phi and psi rotation axes and at multiple points along the bulkhead. Only the Proto machine has the capability to do all of these readings under full automation. Both the TEC Figure (50) and AST Figure (48) systems require manual movement along the bulkhead. This is a significant problem as there are many relevant areas on board ships that are difficult or dangerous to access where requiring a person to consistently change the position of the XRD machine will be impractical.

Sample preparation was considered as a significant issue in the application of this approach to ship structures. Paint on the hull must be evenly removed before readings can be taken Results from previous work showed that surface grinding or other forms of deformation can distort residual stress readings [26]. To accomplish this, the X-ray residual stress system needs to come with an portable electro polishing device. As the ability to contain the electrolyte may be difficult or impractical in some of the desired areas of operation, the used electrolyte must be non-toxic, and it must be able to accurately and consistently be used to remove steel and aluminum materials to accurate depths.

The last major challenge is the general challenge of operating in a marine environment. Currently, the needs for studying residual stress can be met on a ship that is either in port or dry dock so problems dealing with movement or rolling of the ship should be minimal. The device needs to able to be carried by one or two people and fit through a standard Navy watertight door. Also important is the device's ability to handle

loss of power and the power surges both common to marine vessels on shore power. All three of these systems have some sort of UPS capability, and the cooling requirements for the low powered X-ray tubes should all be able to be handled without any modification from standard specifications. Effects of corrosion from sea water and sea salt were considered. It was decided that this issue is best handled by thorough cleaning and dry storage of the device after each use.

C. RESULTS

After several reviews, the following 22 items were decided upon as technical requirements for purchase of a XRD.

1. The purchased device will be a portable XRD capable of taking residual stress measurements on both aluminum and steel structures.
2. Be capable of generating X-rays from chromium, copper, or cobalt tubes with the ability to change between types of tubes on the same device in under 2 hours. Two of the three tubes must be included with the system.
3. Be able to take data for variable 2-theta (2θ) and psi (ψ) angle axes on the same spot in the x-y plane.
    a. θ angle measurements will be recorded on dual, position sensitive detectors with at least a 10 degree arc between 130 and 160 degrees , 2θ.
    b. Psi range will be at a minimum of -45 degrees to 45 degrees with psi oscillation possible.
    c. All measurements and adjustments across these angles will be fully automated.
4. Be able to take variable phi (ϕ) measurements without rotation of the sample, minimum range of 90 degrees.
5. Be able to take measurements as a function of position in the x-y plane.
    a. 100 mm range
    b. 1 mm minimum step size
    c. Automated collection of data for a series of points in the x or y directions.
    d. Device must be secured such that the detector will not unintentionally move more than 1mm per hour under normal ships movement and vibrations at dock.

6. Have demonstrated ability to reliably obtain residual stress data from steel and aluminum specimens. Demonstration can be proven by use of previous reports from the same instrument
7. Capable of beam sizes between 1-2 mm (at least two collimators/apertures of 1 mm and 2 mm in size).
8. Be able to take measurements from both from vertical (on a bulkhead or wall) and horizontal orientation (deck or floor) on both aluminum and steel structures.
9. Be equipped with standards for both aluminum and steel for routine field calibration.
10. Be powered by standard 110 or 220 volt plugs.
11. Be able to survive a loss of power for 10 minutes without sustaining irreparable damage to the machine.
12. All components must though a standard navy water-tight door.
13. The system will comply with all ANSI radiation safety standards for commercial X-ray diffraction equipment.
14. Must include components for radiation shielding for use during portable operation.
15. Must include a laboratory enclosure with an interlock system for radiation safety.
16. Must include accessory equipment for the removal of surface material using electro-polishing.
17. Must include necessary hardware and standards for calibration of instrument in the field.
18. Must include training for 2 operators on use of instrument.
19. Must include analysis software loaded onto a laptop computer.
20. Must include shipping containers appropriate for commercial air transport of portable instrument.
21. Must take delivery within 12 weeks of order.
22. Must include one-year warranty.

THIS PAGE INTENTIONALLY LEFT BLANK

VI. OBJECTIVE #4: DEVELOP CASE STUDY DEMONSTRATING THE NECESSARY STEPS TO PERFORM IN SITU RESIDUAL STRESS MEASUREMENTS ON A USN CRUISER

This section will outline an initial application portable X-ray residual stress measurement on an aluminum superstructure.

A. PROBLEM

Current USN guided missile cruisers have a steel hull and an aluminum superstructure. Significant cracking problems have been found to have occurred on a variety of different decks caused by fatigue cracking, stress corrosion cracking and exfoliation. Figures (53, 54) show cracking from the 03 to 06 decks on the structure. Cracks this high in the structure are of particular interest, as these areas do not have high levels of structural stress on them as exists on the lower parts of the superstructure. There is no single cause of these failures as some are clearly fatigue cracks caused by residual stress from welding and others by stress corrosion cracking. In Figure (53), cracking was most likely caused by multiple modes. Each of these failures is either caused or exacerbated by residual stress from welding, joining or modifying the vessel. Getting accurate and reliable residual stress readings on this ship's structure would help the Navy decide where and how countermeasures, such as laser peening or UIT should be implemented and also help understand the overall impact that additions, changes or repairs make to a vessel and how best to mitigate possible future failures.

Figure 51. Cracking and exfoliation corrosion on aluminum. USN cruiser photo courtesy of W. Goins.

Figure 52. Cracking on USN Cruiser fwd of pilot house. Photo courtesy of W. Goins.

This study will focus on performing XRD residual stress measurements on two different locations on the vessel. The first is shown in Figure (52) on the weather deck forward of the pilot house. Here, there has been cracking near the forward surface in between various antenna and deck fittings. Considering the fact that there have been

multiple welds made in the metal within a few feet of aluminum plate, these cracks are likely due to residuals stress from the multiple welds within a small area. The second spot is the shown in Figure (53) is more clearly a crack caused by residual stress from a weld. The crack runs parallel to a weld line where modifications had been recently made on the deck. Also, the location of the missile system on this replaced part of the deck plate will add additional stress to the metal. These two locations should demonstrate both the measurement of residual stresses from normal manufacturing and wear of the ship for the first location and the stress from welding repair and refitting the ships from the second location.

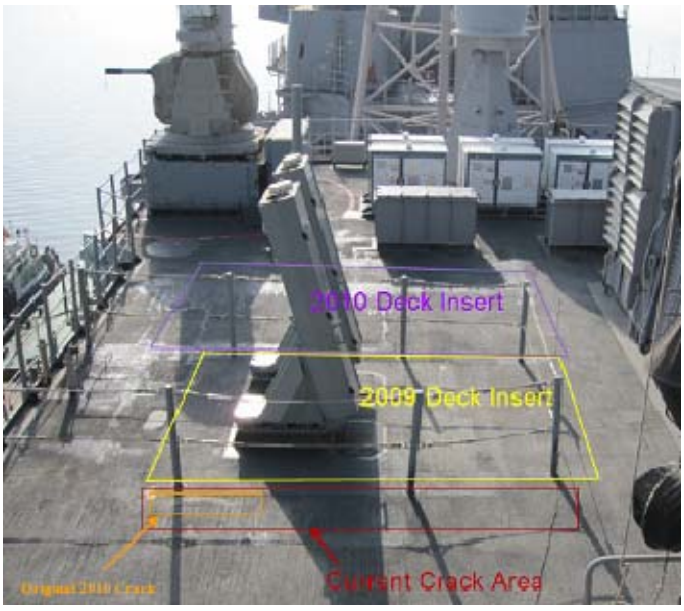

Figure 53. USN Cruiser 04 deck. Crack along welds from deck inserts. Photo courtesy of W. Goins.

B. PREPARATION

One of the primary problems in applying XRD will be the surface preparation. Paint and nonskid coatings must be completely removed from the metal in order to preform XRD measurements. The normal method for removing these coatings would be to use a needle gun on the surface. This approach will lead to a peening or possibly a grinding effect that will change the residual stress readings at the surface. To avoid this

surface stress, a solvent will be applied to remove the paint. Removal of non-skid coatings may be more difficult as using a solvent may not be practical due to the large coating thickness. Here, a physical method to remove the top layers of nonskid will be used, followed by solvents to remove the final layers to the surface of the metal. All measurements will need to be performed at a depth profile of at least .5 mm. For the electro polishing to work properly, the metal surface must be clean and free of any paint or other surfactants that could inhibit the process. The cleaned surface must extend a few inches around the diameter of the measurement spot to ensure that accurate depth measurements can be taken.

The next issue is where exactly measurements should be taken. XRD is an inherently time consuming process with each measurement taking several minutes. Including depth profiling through electro-polishing can add several hours to a given residual stress measurement so carefully choosing the measurement sites is important.

For the first site shown in Figure (54), six locations among the marked yellow lines will be measured to at least four different depths below the, as well as one separate location along the deck away from any deck fittings and welds. These measurements will give a broad stress profile of this area and gain some insight as to why the cracks in this area grow were they do. Of particular interest is whether the damage is caused by residual stress from the large number of local welds or if it is a result of normal stress loading.

For the second site, Figure (55) shows two lines moving transverse from the deck welds, one on the side that is showing the crack and the second on the adjacent side of the deck that was replaced. These measurements should also look at the difference between the transverse and longitudinal residual stresses between the welds as this crack initiated as expected along the higher longitudinal stress gradient of the weld. Doing these measurements on both sides of the replaced deck should give some insight as to why the crack started on the side it did, and whether the residual stress was exacerbated by its location on the deck or by material properties such as the plate orientation.

Figure 54. 04 deck close up of fatige crack with suggested locations of residual stress measurements in yellow. Photo courtesy of W. Goins.

Figure 55. Fwd of pilot house marked with suggested location of XRD residual stress analysis. Photo courtesy of William Goins.

These same measurements should then be repeated on the same or similar area after a peening technique is performed. Our initial testing will use UIT as the peening method. Once the first set of readings is taken, the surrounding area should be peened and then a second set of adjacent residual stress reading should be taken at the same distances

from welds and depths as before. This data can be combined with the Goodman relationships, Equation 4 shown again below, to estimate the change in fatigue life for these structures based upon the measured residual stresses.

$$\sigma_a = \sigma_{fat}\left[1 - \frac{\sigma_m}{\sigma_{ut}}\right] \tag{4}$$

VII. CONCLUSIONS

The objective of this thesis was to study the feasibility of using portable X-ray residual stress measurements onboard active maritime vessels. To support this overall objective, several sub-objectives were met including collecting and assessing the feasibility data on welded aluminum plates, looking at the effects of UIT treatment on residual stress measurements, developing a requirements document for procurement of a portable X-ray diffractometer, and performing a case study of how this method can be used to make field measurements on a Navy cruiser.

Residual stress data from three different portable X-ray diffractometers on aluminum alloys was gathered from manufacturers and analyzed. This analysis found that consistent results were possible, as long as careful consideration was paid to the surface effects, the grain structure, and the orientation of the sample.

X-ray residual stress was successfully performed at NPS using a laboratory diffractometer on ultrasonically treated samples. These 5456 aluminum samples were collected from a Navy cruiser that had been subjected to UIT treatment in the field. Laboratory data compared well with data from a portable X-ray diffractometer on these samples.

A detailed set of technical requirements was written to enable the purchase of a cost effective and practical, portable XRD residual stress analyzer for field use on active navy vessels. Based on these technical requirements, a case study was developed that examined how a portable X-ray diffractometer can be used to take useful residual stress data from a USN cruiser at dock. Areas where cracking has occurred were identified and two different areas with different modes of cracking were selected for study. A set of measurements around the affected areas was planned and the procedure to prepare and execute the study was discussed.

Use of portable XRD technology will soon allow for a detailed understanding of residual stresses aboard active USN vessels. Combining this technology with existing

design tools and finite element analysis will offer a more comprehensive approach for navy engineers dealing with the cracking problems in aluminum structures aboard ships.

LIST OF REFERENCES

[1] H. R. Mattern, "Laser peening for mitigation of stress corrosion cracking at welds in marine aluminum," M.S. thesis, Naval Postgraduate School, Monterey, CA, 2011.

[2] T. Harrison, "Analysis of the FY 2012 defense budget," Center for Strategic and Bugetary Assessments, Washington, DC, 2011.

[3] M. Skillingberg, "Aluminum at sea," *Alumlayout,* pp. 27–33, 1/6/2009.

[4] K. A. Crum, J. M. McMichael, and M. Novak, "Advances in aluminum relative to ship survivability," Alcoa Technical Center, 2011, http://www.alcoa.com/defense/en/pdf/Advances_in_Aluminum_Relative_to_Ship_Survivability.pdf.

[5] A. P. Mouritz, E. Gellert, P. Burchill, and K. Challis, "Review of advanced composite structures for naval ships and submarines," *Composite Structures*, vol. 53, pp. 21–47, 2001.

[6] W. D. Jr. Callister, *Materials Science and Engineering: an Introduction.* York, PA: John Wiley and Sons, Inc., 2007.

[7] T. Lamb, N. Beavers, "The all aluminum naval ship – The way to affordable naval ships," 2010, http://www.alcoa.com/defense/en/pdf/Alcoa_Naval_Ship_2010_UK_INEC_Paper_041410.pdf.

[8] N. E. Dowling, *Mechanical Behavior of Materials Engineering Methods for Deformation, Fracture, and Fatigue*. Upper Saddle River, NJ: Pearson Education, Inc., 2007.

[9] I. N. A. Oguocha, O. J. Adigun, and S. Yannacopoulos, "Effect of sensitization heat treatment on properties of Al-Mg alloy AA5083-H116," *Journal of Materials Science*, vol. 43, p. 4208, 2008.

[10] H. Bushfield and M. Cruder, "Sensitized marine aluminum plate & ASTM Standard specification B928—An update," in *SNAME Section Meeting*, 2006.

[11] R. Schwarting, G. Ebel, and T. J. Dorsch, "Manufacturing techniques and process challenges with CG47 class ship aluminum superstructures modernization and repairs," *Fleet Maintenance & Modernization Symposium 2011: Assessing Current & Future Maintenance Strategies*, San Diego, CA, 2011.

[12] S. Ganguly, V. Stelmukh, et al., "Analysis of residual stress in metal-inert-gas-welded Al-2024 using neutron and synchrotron X-ray diffraction," *Materials Science and Engineering*, vol. 491, p. 248, 2008.

[13] S. Kou, *Welding Metallurgy.* Hoboken, NJ: John Wiley & Sons, Inc., 1987.

[14] M. N. James, D. G. Hughes, et al., "Residual stress and strain in MIG butt welds in 5083-H321 aluminum: As-welded and fatigue cycled," *International Journal of Fatigue*, vol. 31, p. 28, 2009.

[15] S. Benedictus-deVries, A. Bakker, et al., "Fatigue cracked initiation behavior of welded AA5083 in a seawater environment," *Journal of Engineering Materials and Technology*, vol. 126, p. 199, 2004.

[16] A. H. Palmateir and K. H. Frank," Application of ultraxonic impact treatment to in-service signal mast arms," Texas Department of Transportation, Center for Transportation Research University of Austin, TX , Tech. Rep. #FHWA/TX-06/5-4178-01-2, 2005.

[17] M. Liao, W. R. Chen, and N. C. Bellinger, "Effects of ultrasonic impact treatment on fatigue behavior of naturally exfoliated aluminum alloys," *International Journal of Fatigue*, vol. 30, p. 717, 2008.

[18] K. N. Tran, M. R. Hill, and L. A. Hackel, "Laser shock peening improves fatigue life of lightweight alloys," *Welding Journal*, vol. 85, p. 28, 2006.

[19] O. Hatamleh, "A comprehensive investigation on the effects of laser and shot peening on fatigue crack growth in friction stir welded AA 2195 joints," *International Journal of Fatigue*, vol. 31, p. 974, 2009.

[20] I. C. Noyan and J. B. Cohen, *Residual Stress Measurement by Diffraction and Interpretation,* Germany: Springer-Verlag New York Inc., 1987.

[21] P. S. Prevey, *X-ray Diffraction Residual Stress Techniques*, *Metals Handbook, 9th Edition, Vol. 10*. Metals Park, OH: American Society for Metals, 1986.

[22] B. D. Cullity, *Elements of X-ray Diffraction.* Reading, MA: Addison-Wesley Publishing Company, Inc., 1978.

[23] D. S. Huff and KM Lynaugh, "Utilization of root cause failure analysis in the investigation of marine deck fitting failures," *Naval Engineers Journal*, winter edition, pp. 93–99, 2001.

[24] R. D. Brenner and E. B. Pardue, "Research and development to develop a nondestructive evaluation instrument (X-ray diffraction) for measuring residual stress in a wide range of naval aviation materials," Technology for Energy Corporation, Naval Air Command, TEC Report R-87-015, 3 April 1987.

[25] S. P. Farrell, L. W. MacGregor, and J. F. Porter, "Stress analysis on canadian naval platforms using a portable miniature X-ray diffractometer," *Journal of Powder Diffraction*, vol. 25, p. 119, 2010.

[26] B. J. Banazwski, "Using X-Ray diffraction to assess residual stresses in laser peened and welded aluminum," M.S. thesis, Naval Postgraduate School, Monterey, CA, 2011.

[27] Y. Nakayama, T. Takaai, and S. Kimura, "Evaluation of surface residual stresses in cold-rolled 5083 aluminum alloy by X-ray method," *Materials Transactions*, vol. 34, p. 496, 1993.

[28] S. Sougata, J. W. Fisher, B. T. Yen, "Fatigue resistance of welded details enhanced by ultrasonic impact treatment (UIT)," *International Journal of Fatigue*, vol. 25, p. 1239, 2003.

THIS PAGE INTENTIONALLY LEFT BLANK

INITIAL DISTRIBUTION LIST

1. Defense Technical Information Center
   Ft. Belvoir, Virginia

2. Dudley Knox Library
   Naval Postgraduate School
   Monterey, California

3. Dr. Luke Brewer
   Naval Postgraduate School
   Monterey, California